Spring 2020

Damage Evaluation of Rolling Element Bearings for Shipboard Machinery

Brenna Lyn Feirer

DAMAGE EVALUATION OF ROLLING ELEMENT BEARINGS FOR SHIPBOARD MACHINERY

by

Brenna Lyn Feirer

Bachelor of Science in Engineering
University of South Carolina, 2019

Submitted in Partial Fulfillment of the Requirements

For the Degree of Master of Science in

Mechanical Engineering

College of Engineering and Computing

University of South Carolina

2020

Accepted by:

Paul Ziehl, Director of Thesis

Jamil Khan, Reader

Bin Zhang, Reader

Cheryl L. Addy, Vice Provost and Dean of the Graduate School

DEDICATION

It is with genuine gratefulness and warmest regard that I dedicate this thesis to my family and friends. A special appreciation to my loving parents, Marilyn and Ernest Feirer whose encouragement supported me through every step of this process.

I also contribute this thesis to my friends who have supported me throughout this process. Especially Kim Cardillo for the many hours of proofreading.

ACKNOWLEDGEMENTS

I want to thank my committee members who graced me with their expertise and precious time. A special thanks to Dr. Paul Ziehl, my major professor for his hours of reflecting, encouraging, and patience throughout the entire process. Thank you, Dr. Jamil Khan, and Dr. Bin Zhang for serving on my committee.

I would also like to acknowledge and thank the University of South Carolina Mechanical Engineering Department support staff and professors. Lastly, I would like to acknowledge Rafal Anay for his continued support and advise.

ABSTRACT

Rolling element bearings perform an essential role in most all rotating machinery. To prevent degradation to machine performance, unforeseen costs and unexpected system failure, bearing fault diagnosis and prognosis are used. Acoustic Emission (AE) introduces high sensitivity, early and rapid detection of cracking, and real time monitoring that can alarm once cracking is noticed.

The purpose of this research is to nondestructively monitor the crack growth in rolling element bearings in a marine environment and to determine the acoustic emission parameters which embody crack initiation and propagation. The intellectual merit lies in:

1. the signal alarm developed from an AE data pattern recognition method,
2. the damage quantification procedure based on intensity analysis parameters, and
3. the specially made rotating machine test bed to simulate a bearing in use on a submarine.

The gap in current literature addressed a shortage of data and findings on acoustic emission signal alarm notification and use of shipboard machinery parameters for acoustic emission monitoring of rolling element bearings. Four rolling element bearings were tested in a specially made rotating machine test bed at various load and rotation cycles to exemplify shipboard machinery operation at various depths. Acoustic emission data classification was done through pattern recognition and neural network software

(NOESIS). All AE data was clustered using k-means unsupervised method and the lowest correlated features were selected for pattern recognition.

It was concluded that the clustering method used successfully classified crack initiation and propagation. Useful AE parameters for classifying crack initiation and propagation are amplitude, initiation frequency, absolute energy, frequency centroid, peak frequency, and signal strength. With use of intensity analysis, it was determined that the intensity at crack initiation and propagation is much higher than at the final section where failure occurred. Acoustic emission is suitable for remote monitoring of bearing degradation. With the use of signal alarms based upon the clustering method and parameters discussed, one can be notified when a crack is initiating and propagating, and prepare for failure of the bearing. The ability to be notified when cracks are initiating and propagating will prevent unexpected system failure and reduce maintenance cost.

TABLE OF CONTENTS

LIST OF TABLES

LIST OF FIGURES

LIST OF SYMBOLS

HI	Historic Index.
N	Number of hits to time t.
S_{oi}	Signal Strength of ith hit.
K	Empirically derived constant based on material.
S_r	Severity.
J	Empirically derived constant based on material.
S_{om}	Signal Strength of mth hit (based upon magnitude of Signal Strength)
CWT	Continuous Wavelet Transform.
$\psi(t)$	Mother Function.
a	Scale Index.
b	Time Shifting.
$s(t)$	Signal Function.

LIST OF ABBREVIATIONS

AE ..... Acoustic Emission

CWT..... Continuous Wavelet Transform

CHAPTER 1

LITERATURE REVIEW

1.1 Introduction

Rolling element bearings perform an essential role in most all rotating machinery. Their reliability and carrying capacity allow for quality machine performance. However, rolling element bearings do not have an infinite life expectancy. To prevent degradation to machine performance, unforeseen costs and unexpected system failure, bearing fault diagnosis and prognosis are used.

Acoustic Emission (AE) has become one of the paramount bearing condition monitoring systems. Acoustic Emission introduces high sensitivity, as well as, early and rapid detection of cracking. Overall, the ability to detect cracking is vital for all rotating machinery.

There have been many studies investigating the AE response of defective bearings. It was shown that certain AE parameters can detect defects prior to the appearance on the vibration acceleration range for thrust loaded ball bearings (Yoshioka & Fujiwara, 1987). Another study demonstrated the usefulness of some acoustic parameters for the recognition of defects in radially loaded ball bearings at low and normal speeds (Tandon & Nakra, 1990). It was suggested that the area under the amplitude time curve is the principal method to distinguish defects in rolling element bearings (Tan, 1990). It appears from the literature that acoustic emission monitoring of crack growth of rolling element bearings simulated with shipboard machinery parameters and signal alarm notifications have yet to be undertaken.

1.2 Rolling Element Bearing

Rolling element bearings are used in substantial amounts of industrial rotating machinery, especially submarines. These bearings are comprised of an inner race, a set of

rollers separated by a cage, an outer race and sometimes a shield or seal. Figure 1.1 shows a visual representation of the components of a ball bearing. In the case of this thesis, ball bearings are being investigated. Ball bearings exceed in radial load support and have average axial load support amongst other bearing rollers such as cylindrical, tapered, barrel, and needle (Hamrock et al., 2004). This allows for ball bearings to succeed in high-speed conditions while producing low friction.

In rotating machinery, bearings are the most used and are the source of faults in such machinery. For example, in a survey done about medium-voltage induction motors, it was found that bearing faults accounted for 44% of the total failures (Georgoulas et al., 2013; Zhang et al., 2011). Since bearings make up most faults, understanding the types of faults that can occur is necessary.

There are three different types of bearing faults: single point defect, multiple-point defect, and generalized roughness. Single point defects are cracks, and holes that are due to a bearing running for a long period (Cerrada et al., 2018). Cracks and holes in the inner and outer race make up 90% of all rolling bearing faults while only 10% occur in the balls or cage of the bearing (Kateris et al., 2014).

Multiple-point defect is a collection of several point defects. They differ from single point defects because of their quantity and the change in relative amplitudes of the components (McFadden et al., 1985). Generalized roughness faults are when a large area of the bearing becomes irregular, deformed or rough. Common causes of generalized roughness faults are contamination, loss of lubricant, or misalignment (Stack et al., 2004). These three faults can happen to a bearing and it should be recorded which faults occur during a test.

1.3 Acoustic Emission

The American Society for Testing and Materials defines acoustic emission as, "the class of phenomena whereby transient elastic waves are generated by the rapid release of energy from localized sources within a material, or the transient waves so generated" (ASTM E1316, 2006). Acoustic Emission (AE) is a type of nondestructive testing. Nondestructive testing is "the application of physical principles employed for assessing the inhomogeneities and harmful defects without impairing the usefulness of such materials or components or systems" (Raj et al., 2002). Some advantages to nondestructive testing are ability to test directly on a test specimen, repeated checks throughout testing are possible, and most tests are rapid. A couple downfalls to nondestructive testing are measurements are indirectly reliable and must be verified, and only scholars skilled in that field can interpret the data.

AE sensors are piezoelectric crystals mounted on a testing specimen. Piezoelectric crystals generate an electric charge when they are compressed or struck. The AE waveform created from this strike is called a hit. These transient elastic waves hold a multitude of properties that are used to filter and cluster data sets. Some of those properties being: signal amplitude, duration, rise time, signal strength, signal energy, count, and frequency. Figure 1.2 shows a typical waveform with different waveform properties.

Signal amplitude is the magnitude of the highest voltage attained by a waveform from a single hit. Hits with a lower signal amplitude normally are considered background noise (Drummond et al., 2007). So, these types of hits can be removed to focus on data that will be more informative about fault propagation. The duration is the time between the AE signal crossing the first and last threshold. Rise time is the time between signal start and

the peak amplitude of that hit. If a hit has an abnormally short or long duration or rise time, it is an indicator of a poor hit.

The signal strength is the measured area of the amended AE signal. A significant jump in signal strength could indicate a fault. Signal energy is the energy within a burst signal. The count of a hit is the number of times a signal passes the threshold. Frequency is the number of cycles per second of pressure variation in a hit (ElBatanouny, 2012). Some other types of frequency are average frequency, peak frequency, and initiation frequency. All these properties of a hit can be used to better cluster and filter data based on an experiment's scope.

Three different contact fatigue stages have been identified, those being run-in phase, permeant-wear phase, and wear-out phase (Zykova et al., 2006). The run-in phase occurs at the beginning of the test and shows and increases in AE activity. When there is a reduction of AE events and becomes stable, the permeant-wear phase begins. The wear-out phase arises when AE activity increases rapidly up to failure. These contact fatigue stages were also identified in a couple other papers (Baby et at., 2006; Fiala et al., 2011; Mazal et al., 2011;Muravaev et al., 2008).

An extensive amount of research has been done on vibrational signal processing for bearing fault detection (Zarei & Poshtan, 2007; Immovilli et al., 2009; McInerny & Dai, 2003). Acoustic Emission signal fault detection has become a fault detection method more enticing than vibrational signal processing. AE signals are more insensitive to noise and disturbances caused by different operation conditions than that of vibrational signals. AE can also offer earlier fault detection than vibrational signals because of its sensitivity to

fault size (Niu et al., 2019). Because of these advantages, AE signal processing is more applicable for bearing fault detection.

1.4 AE Data Filtering

To extract the most pertinent information for the scope of an AE project, one can use data filtering. AE data that is usually not pertinent to fault detection are noise, wave reflections, and friction. To reduce these non-pertinent hits, a quite testing area was upheld, and grease was applied evenly around the test bearing. Even with these precautions, noise from operating the motor and wave reflection will still be detected. Therefore, data filtering was the best course of action. Some data filtering techniques are front end-filtering, pass filtering, D-A (Swansong II filtering), and wavelet analysis.

1.4.1 Front End-Filtering

Front End-Filtering is when a hit is either accepted or rejected based on a predetermined hit property range. Some properties that a front end-filter accepts, or rejects are signal amplitude, energy, counts, duration, rise time, etc. For example, a front end-filter is set to reject any hits that are below a signal amplitude of 40 dB. So, if a hit has a signal amplitude of 38 dB it will be rejected and not recorded, but if it has a signal amplitude of 45 dB it will be accepted and recorded in the data for said test.

Front End-Filtering allows a user to cut out data simultaneously during testing. Unfortunately, if a user sets a front end-filter then wants to access data from the rejected range they would be unable to do so. Front End-Filtering is great for reducing large portions of data that is known to be not useful for the scope of a project.

1.4.2 Pass Filtering

Pass filters focus on the frequency property of waveforms. Three different types of pass filters are low-pass, high-pass, and band-pass. Low-pass filters pass signals with a frequency lower than a preselected cutoff frequency. High-pass filters pass signals with a frequency higher than a preselected cutoff frequency. Low-frequency noise components are deemed to be not correlated with specimen's condition hence useless for data analysis (Jemielniak, 2001). High-pass filters cut out these low nonessential frequency signals. Band-pass filters utilize low-pass and high-pass filters to select a range of frequencies. The band-pass filters allow the user to cut out noisy low-frequency unimportant data as well as outlying spikes in frequency.

1.4.3 D-A Filtering (Swansong II)

D-A Filtering meaning duration-amplitude filtering is a filter used by the masses to cut out noise related external sources and reflections (Tinkey et al., 2002). Some of the external sources can be due to noises created by running a motor or friction between two moving objects. This form of filtering is based on the belief that noise has a low amplitude and long duration. This external emission can be viewed on a graph of amplitude versus log duration in Figure 1.3.

To determine what criteria should be used for the Swansong II filter, Tinkey created a table depicting when data should be cut off based on the "tell-tail" hit. This table is shown as Table 1.1. R-A filtering has been used with Swansong II Filters to further improve the filtering method. R-A filters are used similarly to D-A filtering (ElBatanouny et al., 2014; Anay et al., 2016). It is believed that low amplitude and high rise time are noise hits. The

combination of D-A and R-A filtering may further reduce external emissions than just D-A filtering.

1.5 AE Pattern/Damage Recognition

Once the data is filtered to a point where excess emission has been disregarded, it is time to evaluate the data. A variety of evaluation methods can be used to determine when and how severe damage is. Some of these evaluation methods are intensity analysis, cumulative signal strength, clustering, and signal alarms. These methods are further discussed below.

1.5.1 Intensity Analysis

Intensity analysis is a way to evaluate the structural significance of AE signals and the degree of deterioration of a structure. Intensity analysis utilizes historic index (HI) and severity (S_r). The historic index is a trend analysis that approximates the change of slope in signal versus time by comparing the signal strength of the prior hit to a value of collective hits (ElBatanouny, 2012). Eq (1.1) shows the formula used for historic index (ElBatanouny, 2012).

$$HI = \frac{N}{N-K}\left(\frac{\sum_{i=K+1}^{N} S_{oi}}{\sum_{i=1}^{N} S_{oi}}\right) \quad (1.1)$$

Where,

HI: Historic Index

N: Number of hits to time t

S_{oi}=Signal Strength of *i*th hit

K=Empirically derived constant based on material

The value of K was selected to be a) N/A if N≤50, b) K=N-30 if 51≤N≤200, c) K=0.85N if 201≤N≤500, and d) K=N-75 if N≥501. Severity (S_r) is the average signal strength for

several events with the largest value of signal strength (Golaski et al., 2002). The formula for severity is found in Equation 1.2.

$$S_r = \frac{1}{J}\left(\sum_{m=1}^{J} S_{om}\right) \quad (1.2)$$

Where,

S_r: Severity

J: Empirically derived constant based on material

S_{om}: Signal strength of *m*th hit (based upon magnitude of signal strength)

Once these values are calculated they are plotted onto a severity vs historic index chart called an intensity plot. The intensity plot is divided into sections depending on the level of damage occurred. The intensity values of less significance are plotted near the bottom left of the plot while the values of high significance are found in the top right corner (Fowler et al., 1989).

These sections can be adjusted based on structural properties of the specimen. An example of an intensity chart from a bridge can be found in Figure 1.4 (Shahiron et al., 2012). In this figure, section A is insignificant AE. Section B presents minor surface defects like pitting. Section C presents defects that require more in-depth evaluation but are not overly sever. Section D presents significant defects but are not the most sever. Section E holds the most sever defects and immediate shut-down is needed. Note that these section ranges and meanings will change based on the specimen used. Research analysis has been done using intensity analysis on bridges (Shahiron et al., 2012; Golaski et al., 2002; Lovejoy et al., 2008; Anay et al., 2016), but this analysis can be useful in a wide range of acoustic emission testing.

1.5.2 Cumulative Signal Strength

Cumulative Signal Strength (CSS) is defined as the integral over time of the rectified signal (Mangual et al., 2012). In a plotted CSS vs time graph, it is important to note when there is a large spike in the CSS. This means that there is possible damage at that time. CSS is reliable because it depends only on the parameters of amplitude and duration. CSS is a very helpful form of analysis because it allows the researcher pinpoint when damage could have happened and allows them to focus on smaller portions of data than assess all points in time that may pertain to damage. CSS is used in the monitoring and analysis of a wide variety of materials including concrete (Shahidan et al., 2013) and composites (Kumar et al., 2017). CSS also plays a major role in intensity analysis.

1.5.3 Clustering

Clustering is a pattern recognition process. This is where regularities or significant features in data are recognized and categorized into classes. The three parts in clustering are data perception, feature extraction, and classification (Abdelrahman, 2016). The features extracted in acoustic emission signals are the waveform parameters (amplitude, frequency, rise time, etc.). To classify these features, one can use supervised or unsupervised pattern recognition.

Supervised pattern recognition is where a set of training data with predefined classes is used to train a classifier to perform as effectively as possible (Farhidzadeh et al., 2014). This type of pattern recognition is helpful when a type of damage is known in advance. There is a wide variety of supervised classifier algorithms based on the complexity of a project and the speed performance needed for the classifier. For AE data, examples of

supervised classifier algorithms would be K-Nearest Neighbor's method (K-NN) (Cover & Hart, 1967), linear classifier, and Neural Networks (Anastasopoulos, 2005).

Unsupervised pattern recognition is where data is classified into clusters based solely on their features and similarities between them. With unsupervised pattern recognition, there is no previous knowledge on damage type nor is it required. The user plays a major role in classifying these clusters because they must decide what feature to use and how to relate those features. It can be helpful for the user to create a correlation matrix and correlation hierarchy diagram. This matrix and diagram will allow the user to view the highest and lowest correlated features. The lowest correlated features should be chosen to determine the clusters so that the clusters differentiate greatly (Mitra et al., 2002). Standard unsupervised clustering methods are k-means algorithm (Likas et al., 2003) and principal component analysis (PCA) (Gutkin et al., 2011). The k-means algorithm creates clusters based on similar instances in terms of Euclidean distances between the instances and their cluster centroid (Yasami & Mozaffari, 2010).

1.5.4 Continuous Wavelet Transform (CWT)

The continuous wavelet transform is used to linearly decompose a signal into wavelets. It is constructed from the sum over the signal time multiplied by a mother function. A mother function is a scaled and shifted version of the wavelet function (Baccar & Söffker, 2015). The wavelet transform can be obtained by Eq(1.3) below.

$$\mathrm{CWT(a,b)} = \frac{1}{\sqrt{|a|}} \int s(t)\psi\left(\frac{(t-b)}{a}\right)dt \quad a \neq 0 \qquad (1.3)$$

Where,

$\psi(t)$: Mother function

a: Scale index

b: Time shifting

s(t): Signal

As seen above the wavelet transform is a function of time and frequency. So, CWT allows the discovery of how a signal's frequency content evolves in time. This is quite helpful when detecting and classifying damage signals. Events that are localized in time and frequency indicate a possible signal due to damage.

1.5.5 Signal Alarms

Signal alarms are not a post processing damage recognition technique. Signal alarms are used to notify the researcher in the experimental process when a set of features have happened in a hit. This is very helpful for researchers needing to physically stop an experiment and check the condition of a specimen due to damage. The AEwin software can do three different types of alarms: average signal level alarm, cluster alarms, and multivariate alarms. The average signal level alarm notifies the user when a hit is out of the users predetermined signal range. A cluster alarm allows the user to define a cluster grading and be notified when the cluster analysis enters that grading level (Schultz et al., 2014).

Lastly, multivariate alarms are where the user defines a range for as many features as desired, once all those features are contained in one hit an alarm will activate. Signal alarms are saved within the data file so the alarm can be found and accessed after and during an experiment. Signal alarms have been used in the recognition of early stages of cracks in rotating gearbox components (Xiang, 2017). Accessible literature indicates that acoustic emission monitoring of damage and prognosis of rolling element bearings is promising.

Table 1.1 Swansong II Filtering based on “Telltale” Hit (Tinkey, 2002)

Amplitude		Duration
< 5 dB plus the Threshold	And	> 2 milliseconds
	- Or -	
< 10 dB plus the Threshold	And	> 3.5 milliseconds
	- Or -	
< 15 dB plus the Threshold	And	> 4.5 milliseconds

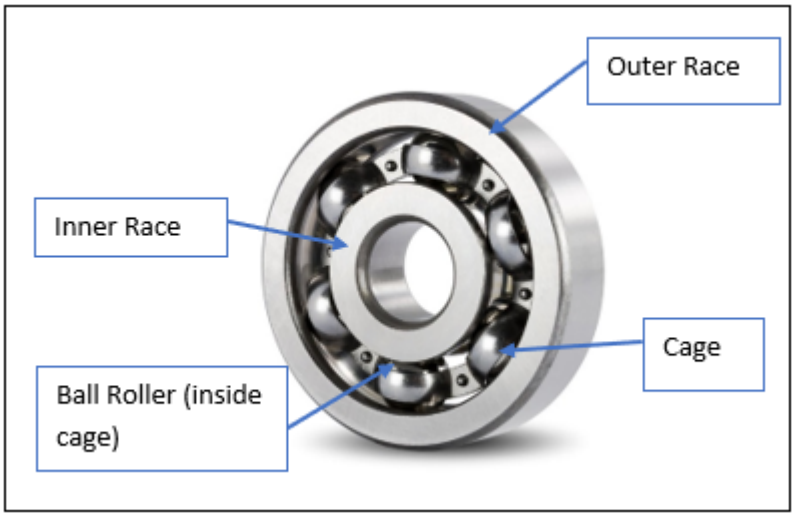

Figure 1.1 Ball Bearing Components

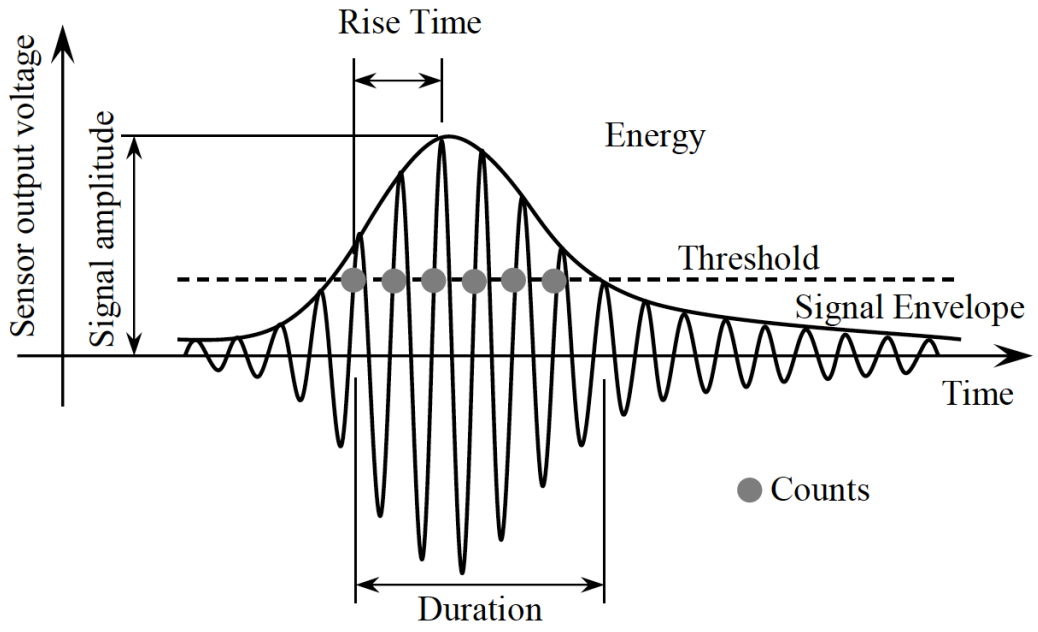

Figure 1.2 Waveform Properties (Xu, 2008)

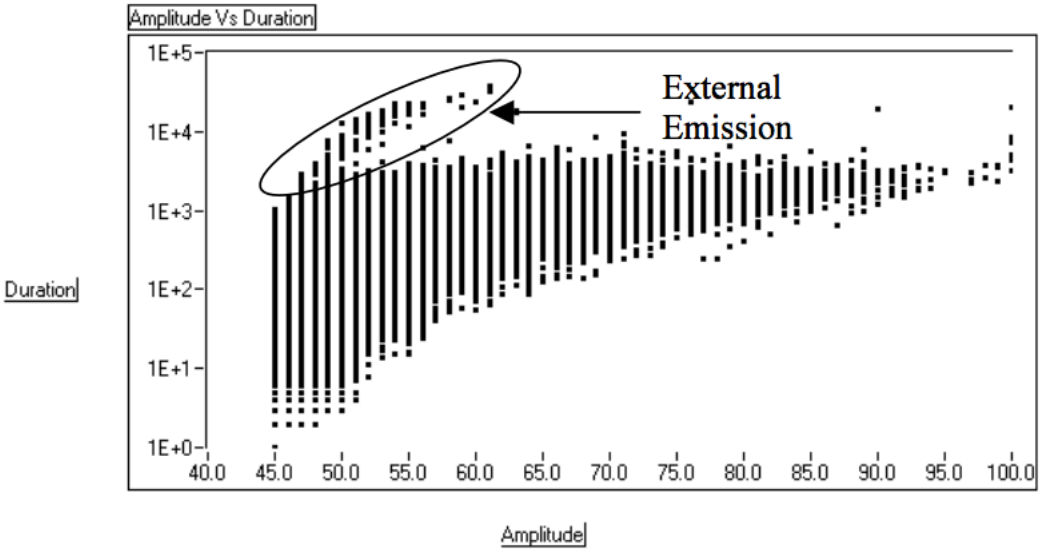

Figure 1.3 Amplitude vs Log Duration (Tinkey et al., 2002)

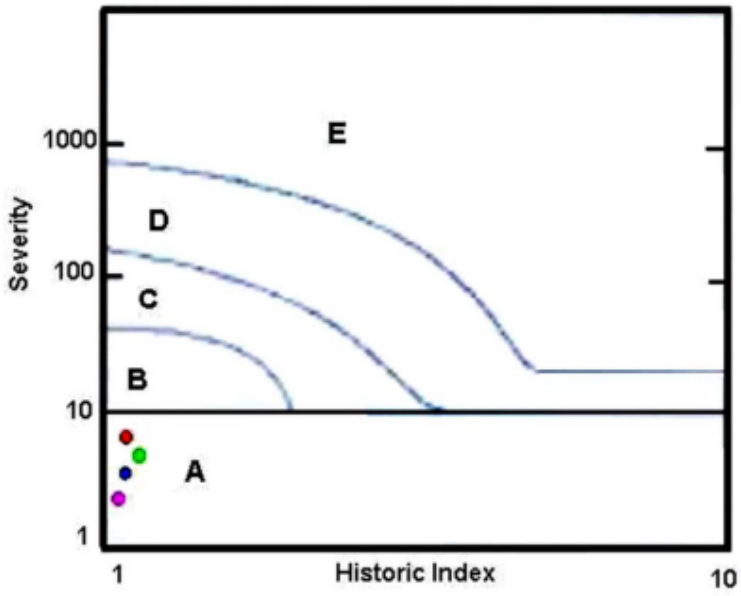

Figure 1.4 Intensity Plot for Typical Bridge (Shahiron et al., 2012)

CHAPTER 2

EXPERIMENTAL SETUP

2.1 Introduction

To simulate a bearing in use on a submarine, a rotating machine test bed was designed. This machine was designed to run a bearing to failure while recording diagnostic data. The test bed components were inspected regularly to ensure ongoing functionality and prevent machine failure during an experiment. The machine ensures that a bearing may be rotated at high speeds while enduring a downward force of up to 4000 pounds through a hydraulic system. Acoustic emission data was collected during the experiments by a Sensor Highway II data acquisition system.

2.2 Rotating Machine Test Bed

The rotating machine test bed is composed of an electric motor, variable frequency drive, hydraulic press system, support bearings, test bearing, shaft/motor coupler, and an acrylic shield. Table 2.1 includes all the instrument specifications. These components are shown in Figures 2.1 and 2.2. Figure 2.1 shows the rotating machine test bed without the shield while, Figure 2.2 depicts how the shield is placed. It is important that during operation all bystanders remain behind the shield.

2.2.1 Electric Motor

The Dayton 2 HP General Purpose Motor, 3-Phase, 3450 RPM, Voltage 230/460, Frame 56H was used. It was chosen for its reliability, controllability, and reduced noise compared to other motors. The system wiring spans from a power source to the motor chassis. Between these systems is a power switch and variable frequency drive (VFD). It is important to note that the motor and VFD each hold a ground wire to ensure safety.

2.2.2 Variable Frequency Drive

To ensure the motor can be controlled externally through a microcontroller, a VFD was used. The Teco Westinghouse L510-101-H1-U VFD can trigger a current protection of 4.2 amps at around 24 Hz. This VFD can operate in a manual speed setting or present speed cycling. The speed cycles used in this experiment were cycles of 10 Hz, 15 Hz, 20 Hz every minute, and 15 Hz, 20 Hz every two minutes.

2.2.3 Hydraulic Press System

The hydraulic piston is connected to a hydraulic pump through a hydraulic line. The internal surface of the piston is one square inch therefore, the conversion from psi to applied piston force is 1 to 1. The hydraulic pump can apply 10,000 psi to the hydraulic system. In this experiment, the hydraulic pump applies a psi of either 625, 1250 or 1875 to the bearing housing. A gauge showing the pressure reading is mounted on top of the hydraulic pump and a pressure release valve is located next to it. The release valve is turned counterclockwise to remove pressure from the system. The hydraulic fluid will leak from the pump if the release valve is left opened or significantly loosened.

2.2.4 Test Bearing

The machine is configured to handle bearings with an inner diameter of 25 mm and outer diameter of 52 mm. The bearings used for this experiment are BL 35JA19 radial ball bearings. This ball bearing utilizes double rubber seal and can withstand a dynamic load of 3,150 pounds and static load of 1,770 pounds. The runners are composed steel. The bearing can go at the maximum speed of 15,000 rotations per minute (RPM) when lubricated with grease.

2.2.5 Shaft/Motor Coupler

The shaft/motor coupler transfers a rotation force from the motor shaft to the machine shaft. The coupler has a dampening system to reduce vibration and provide flexibility to compensate for misalignment. To preserve the coupler, alignment should be as close as possible. The damping component can become worn which can cause excess vibration. At the connection point, the motor shaft has a diameter of 16 mm and the bearing shaft has a diameter of 20 mm as seen in Figure 2.1.

2.2.6 Acrylic Shield

The acrylic shield is the most necessary part of the mechanism. The shield must always be up when the machine is in operation. If bearing or coupler failure occurs during operation, the shield protects users form potential shrapnel.

2.3 Acoustic Emission Data Acquisition System

To acquire acoustic emission data generated from the rotating machine test bed, an acoustic emission data acquisition system (Figure 2.3) was utilized. A 16-channel Sensor Highway II (SHII), manufactured by MISTRAS Group, Inc. (Princeton Junction, NJ, USA), was utilized as the data acquisition system. The sensor sensitivity was checked by applying Hsu-Nielsen sources (Pencil Lead Break) (Boczar & Lorenc, 2004) before and after each experiment. If the difference between two sensors is more than ±3dB the system should be reevaluated.

2.3.1 AE Sensors

Four B1025 broadband sensors from Digital Wave Corporation were used in this experiment. The operating frequency range of these sensors is 50-2000 kHz. They were

attached around the bearing housing to acquire data from all portions of the box (Figure 2.4).

Double bubble epoxy was used as the coupling agents to fix the sensors on the bearing housing. It is important to use an adhesive that is not greatly affected by heat. The bearing housing will begin to heat up after long run times which can affect the adhesive. After the sensors are securely connect to the housing, they are attached to preamplifiers.

2.3.2 Preamplifiers

Four AE signal preamplifiers (type 2/4/6, MISTRAS Group) were used in this experiment which are switch selectable gain single ended and differential preamplifiers. They were supplied with 20/40/60 dB gain (40 dB was used) and plug-in band pass filters from 100 to 1200 kHz. This gain increases the signal level to be more visible in the data acquisition system. The preamplifiers are connected to the data acquisition system by coaxial cords.

2.3.3 Data Acquisition System

Sensor Highway II data acquisition system from Physical Acoustics Corporation was used. In combination with the AEwin for Sensor Highway Smart Monitor, all the acoustic emission data is obtained and displayed in real time. The AEwin software (Physical Acoustics Corporation, 2007) allows for a variety of filters, graphs, and signal alarms to be set.

2.4 Operation

The operational steps for the acoustic emission system can be seen below.

1. Open AE software.
2. Create new layout.

a. Sampling Rate:1 million samples per second
b. Timing Parameters (based on investigation to ensure 1 quality waveform in each hit):
    i. Peak Definition Time(PDT): 200 microseconds
    ii. Hit Definition Time(HDT): 800 microseconds
    iii. Hit Lockout Time(HLP): 1000 microseconds
c. Threshold: 45dB (based on background noise tests)

3. Do a PLB test.
4. Conduct background noise check. To do this start a test without running the mechanism or touching the mechanism in any way. If there are any hits in this test, then there is too much background noise.
5. Conduct a no force test. This is where you run a test without any pressure on the bearing housing from the hydraulic press. Run for 10 minutes to get a baseline of how loud the machine test bed is. This will be helpful when determining what filtering should be used.
6. Set signal alarm at predetermined or inferenced properties to notify when a possible crack will happen.
7. Finally, you will be able to begin an actual test. It is important that there is someone always watching the machine when it is running. When there is a signal alarm it is important to stop the test, take out the bearing, and document any changes in the bearing. A microscopic camera may be helpful with the minute cracks.

The operational steps for the rotating machine test bed is described below. It is important to follow these steps to ensure safe usage.

1. Check the following:
    - Switch is in the off position.
    - VFD and motor are correctly grounded.
    - There are no loose connections or shorts in the electrical system.
    - Acoustic sensors are on the bearing housing before start-up.
    - Bearing housing is centered under the hydraulic piston to correctly transfer force.
    - The motor/shaft coupler is secure.
    - There are no loose objects near the machine.
    - All parts have been correctly reassembled after disassembly.
2. Power the machine on by flipping the power switch.
3. Configure the VFD for the experiment.
4. Pressurize the hydraulics to the desired force for the given experiment. This should be done before starting the machine unless the desired force exceeds the static load rating of the bearing.
5. Start the machine by pressing the run button on the VFD.
6. Begin recording data after the machine starts to avoid undesired start-up noise at the beginning of the experiment. The recording program can also be stopped before the machine is stopped to avoid recording the shutdown of the machine.
7. Stop the machine by pressing the STOP/RESET button on the VFD.

8. Release hydraulic pressure by turning a knob on the side of the hydraulic pump. Re-tighten this knob after depressurization to prevent oil from leaking out of the hydraulic pump.
9. Analyze the bearing.
10. Process the data for diagnosis and prognosis of the test bearing.

Using the above operation steps four bearings were tested. The first bearing was tested with a load of 625psi with a rotation cycle of 1 minute at the following rates: 10Hz, 15Hz, and 20Hz. The first bearing took approximately 26 hours to fail. The next two bearings were tested with a load of 1250psi with a rotation cycle of 2 minutes at 15Hz and then 2 minutes at 20Hz. The last bearing was tested with a load of 1875psi with a rotation cycle of 2 minutes at 15Hz and then 2 minutes at 20Hz. This change in load and rotation cycle is due to further analysis of shipboard machinery operation at various depths. 650 psi hydrostatic pressure is experienced at 1500ft, but at deeper depths such as 2000ft and 2900ft the hydrostatic pressure increases to a range of 974psi to 1,252psi (Liang, et. al. 1998). To accelerate the degradation process, higher loads and heightened rotation cycles were used.

Table 2.1 Instrument Specifications

Instrument	Model
Electric Motor	Dayton 2 HP General Purpose Motor, 3-Phase, 3450 RPM, Voltage 230/460, Frame 56H
Variable Frequency Drive	Teco Westinghouse L510-101-H1-U VFD
Hydraulic Press System	Strongway 10 Ton Hydraulic Ram Pump and Strongway 2 Ton Hydraulic Mini Ram
Test Bearing	BL 35JA19 Radial Ball Bearing, Double Shielded Bearing Type, 25mm Bore Dia., 52m
Shaft/Motor Coupler	16mmx20mm Shaft Aluminum Alloy Motor Flexible Plum Coupling Coupler
Acoustic Emission Data Acquisition System	16-channel Sensor Highway II (SHII) from Physical Acoustics Corporation
AE Sensor	B1025 broadband sensors from Digital Wave Corporation
Preamplifiers	Signal preamplifiers (type 2/4/6, MISTRAS Group

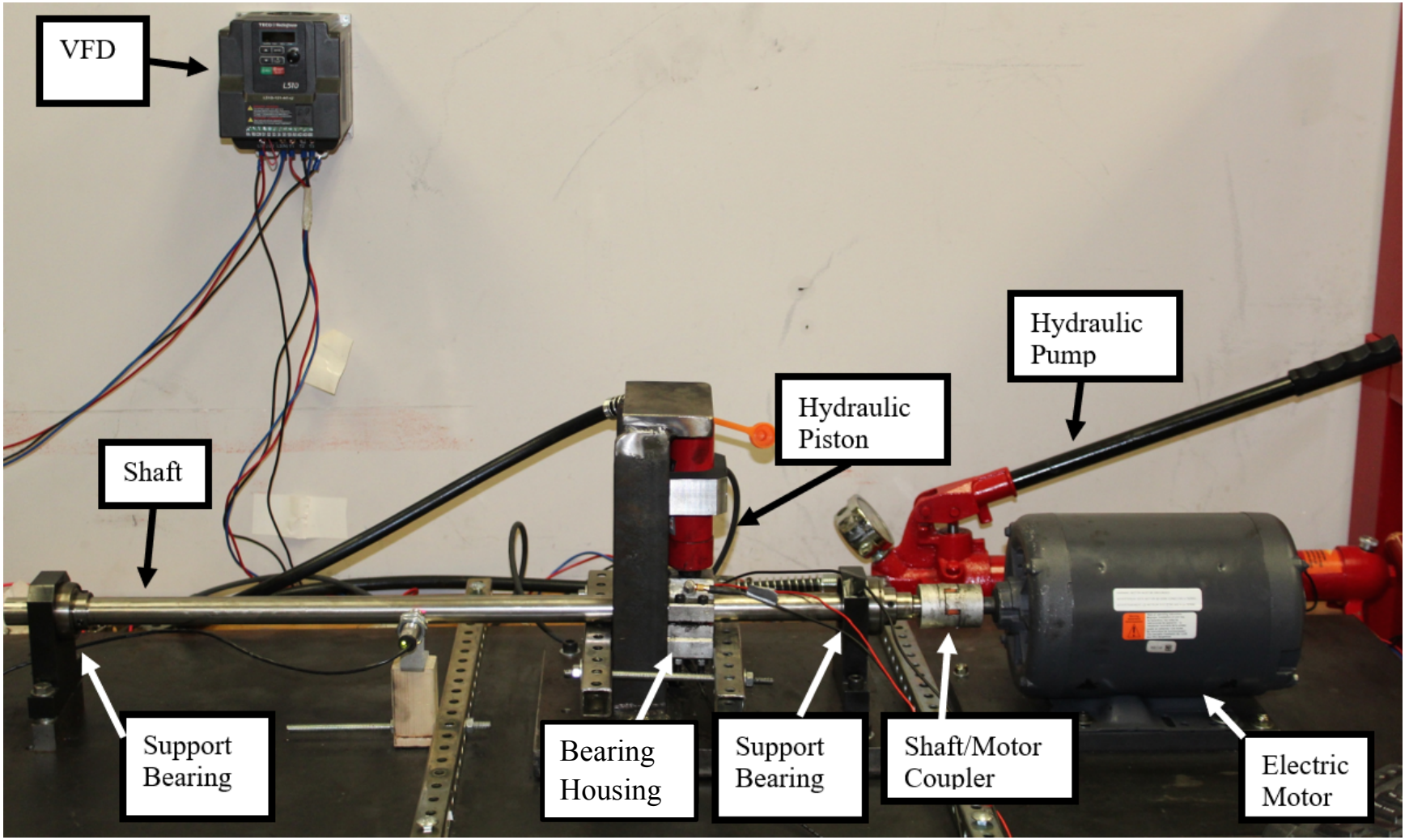

Figure 2.1 Rotating Machine Test Bed without Shield

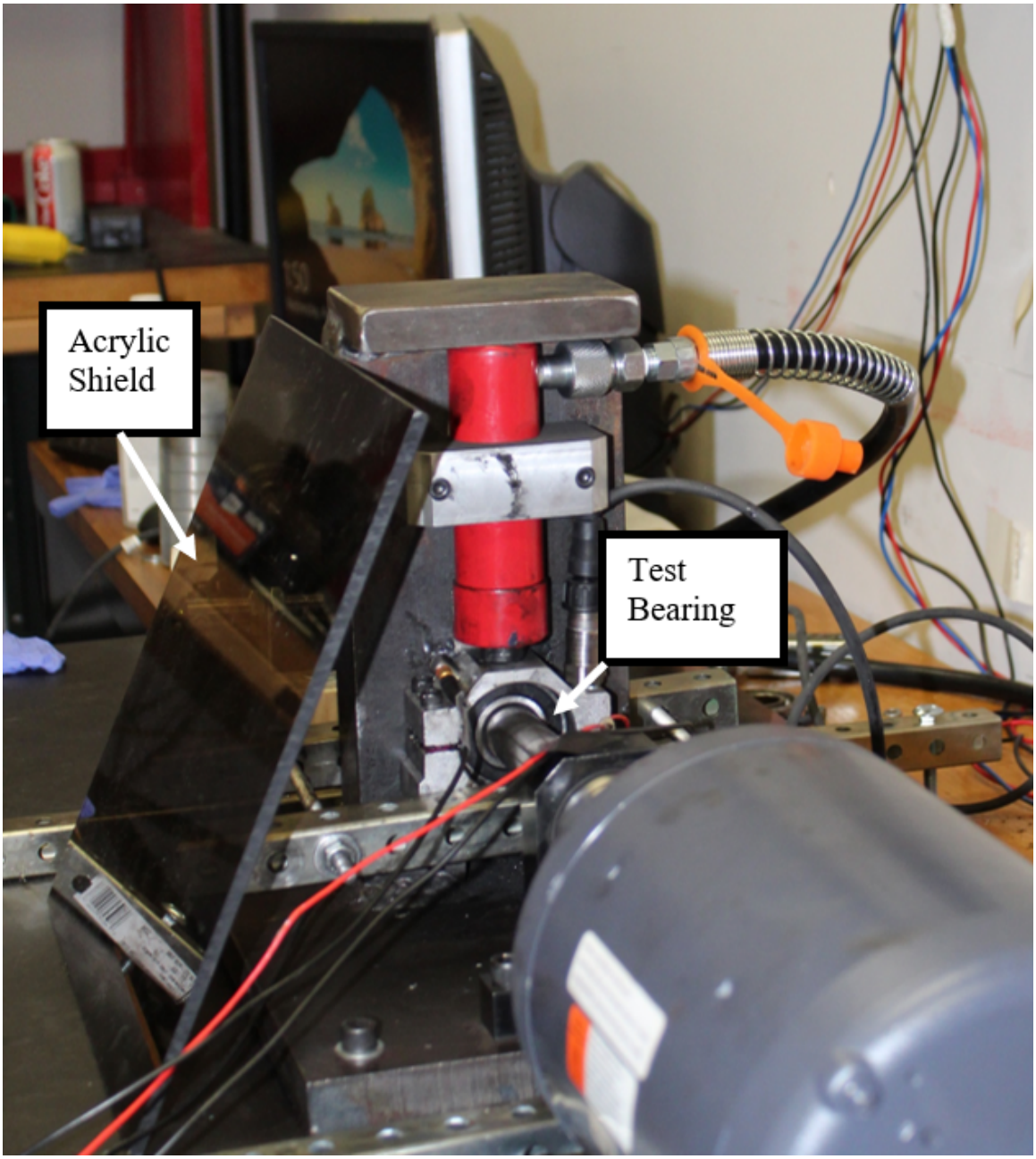

Figure 2.2 Rotating Machine Test Bed with Shield

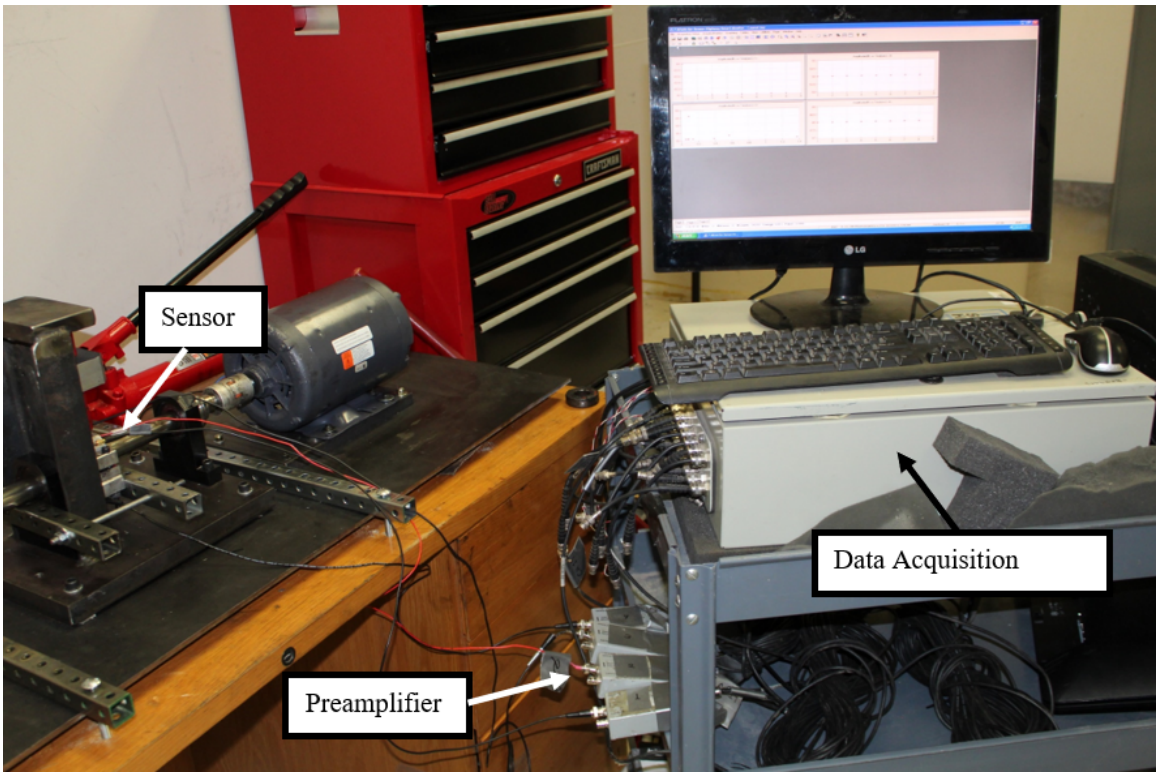

Figure 2.3 AE Data Acquisition Setup

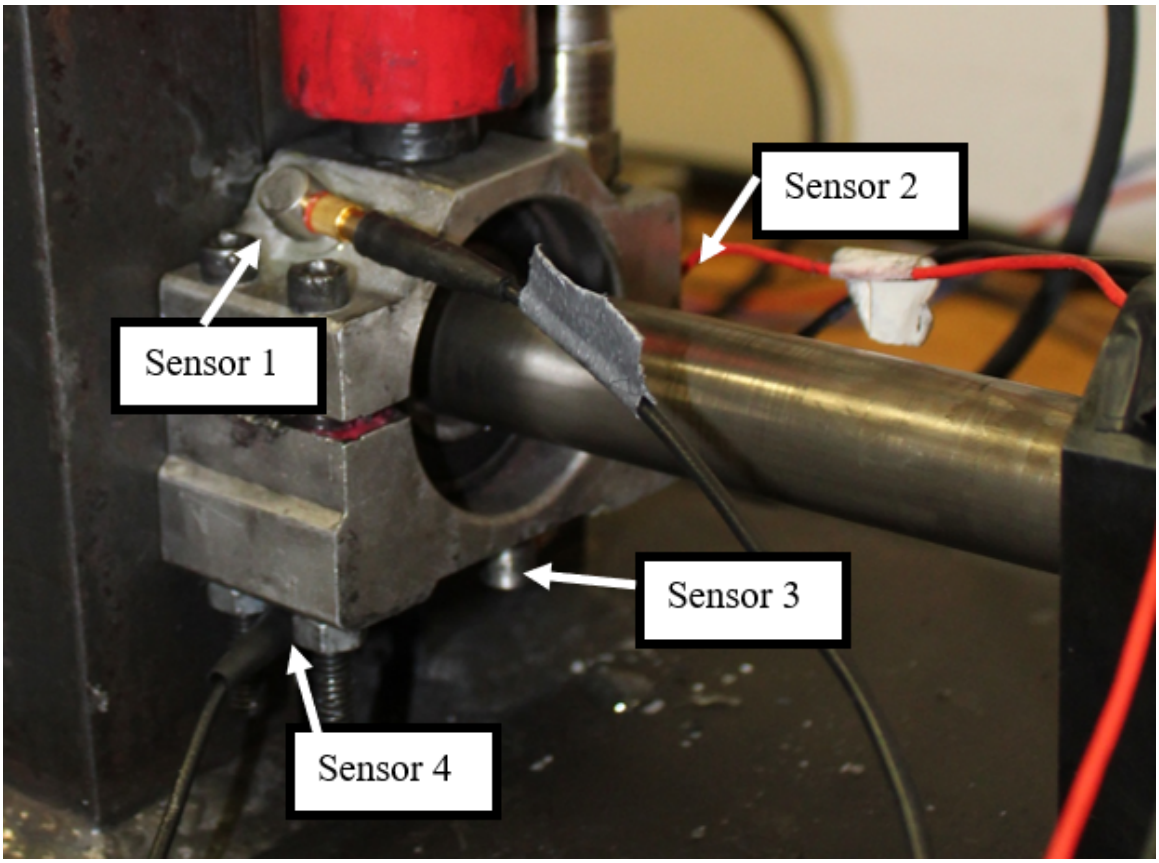

Figure 2.4 Sensor Formation

CHAPTER 3

ANALYSIS

3.1 Introduction

Four tests were done in order to classify crack growth of BL 35JA19 ball bearings. For each test, a new bearing with no detectable deformities was placed into the rotating machine test bed and run at various rotation cycles and loads (Table 3.1). The nondestructive monitoring technique used was acoustic emission. The acoustic emission data from each test was filtered by front end amplitude filters. These filters were chosen to have an amplitude of 60 dB based off the no force test. This filter removes environmental noise from being collected. Such data was then analyzed for each test.

The data was analyzed by cumulative signal strength (CSS), k-means unsupervised clustering, continuous wavelet transform (CWT), and intensity analysis. The k-means unsupervised clustering was achieved by creating a correlation hierarchy diagram. Through the hierarchy diagram, it was determined that the lowest correlated features were rise time, energy, amplitude, average frequency, reverberation frequency, initiation frequency, absolute energy, frequency centroid, and peak frequency. These features were entered into the pre-process features, then the k-means unsupervised method with distance type of Euclidean was used to create three different clusters. This clustering method was used for all tests. In this chapter, the analyzed data will be presented and discussed for each test. The results from each test will then be compared to one another.

3.2 Test 1 Analysis

The ball bearing was run to failure with a rotation cycle of 10 Hz, 15 Hz, and 20 Hz and a pressure of 625 psi. Each frequency was run for a minute long. It took a total of 25.8 hours for such bearing to fail. Failure occurred at the inner race as seen in Figure 3.1.

The failure was catastrophic, and the inner race was split in half and stuck onto the shaft (boxed in red in Figure 3.1).

The three clusters for Test 1 are shown on the amplitude vs time and signal strength vs time graphs in Figures 3.2 and 3.3, respectively. Clusters 0, 1, and 2 are further explained in Test 2 Analysis. There are two major spikes in signal strength on the graphs which indicates damage. It is evident that there is a small degree of damage on the bearing within the first two hours and no damage was incurred until approximately two hours prior to failure.

3.3 Test 2 Analysis

After Test 1, the pressure was increased to 1250 psi and rotation cycle to 15 Hz, and 20 Hz. Each frequency was run for two minutes long. The change in load and rotation cycle was chosen based on further analysis of shipboard machinery operation at various depths. At deeper depths, such as 2000 ft and 2900 ft, the hydrostatic pressure increases to a range of 974 psi to 1,252 psi. The increase in load and rotation cycle accelerated the degradation process and the bearing failed after 16.9 hours. Failure occurred at the inner race once again. The failed inner race can be seen in Figure 3.4. The amplitude vs time and signal strength vs time graphs for Test 2, which include the 3 different clusters, are shown in Figure 3.5 and 3.6 respectively. Figure 3.6 displays five spikes in signal strength which is 3 more spikes than Test 1. This is likely due to the increase in rotation cycle and load.

To further analyze each cluster, the waveforms and continuous wavelet transform for every cluster were investigated. The waveform and CWT for each cluster can be seen in Table 3.2. Cluster 0 has noisy waveforms and no localized events in CWT. Cluster 1 also has a noisy waveform but the CWT of cluster 1 is slightly more localized unlike cluster

0. Cluster 2 is related to damage initiation and growth due to the localized event in terms of time and frequency of the CWT and a quality waveform. A localized event in CWT indicates high energy and a meaningful event.

3.4 Test 3 Analysis

Test 3 has the same rotation cycle and load as Test 2. The test was stopped after 15.15 hours due to a loud emission of noise. Little damage was seen on the runners but after further examination, there were minute defects on the balls of the bearing. The same filtering and clustering methods were used on Test 3 as in all other tests. The amplitude vs time and signal strength vs time graphs with clusters can be seen in Figure 3.7 and 3.8. These figures show no heighted amplitude or signal strength at failure for Test 3. This failure reaction is different than Tests 1 and 2 because the failure was due to the balls and not the runners. Even though the failure area is different, there is still about five spikes in signal strength like Test 2.

3.5 Test 4 Analysis

A higher pressure of 1875 psi was introduced and the spikes in data due to damage initiation were validated with pictures throughout the time of testing. The photos of the bearing were taken with a high-resolution camera and a USB microscope camera was used to detect minute surface damages. This test was run for a total of 38.01 hours.

The same filtering and clustering methods were like the other tests. The amplitude vs time and signal strength vs time graphs with classified clusters for Test 4 can be found in Figures 3.9 and 3.10, respectively. On Figure 3.9 dashed lines in various colors were used to denote when photographs were taken of the bearing. These colors coincide with the bordered images outlined in their respective color in Figure 3.11. These images show

a major outer runner damage increase. To clearly see the crack growth as related to signal strength, Figure 3.12 was created. Figure 3.12 shows that large spikes in signal strength correlate with increases in crack growth.

3.6 Compiled Tests Analysis

The four different tests show that jumps in signal strength correlate to crack growth, therefore all the tests are compared using CSS, and intensity analysis. The CSS of each test has been compiled onto Figure 3.13. It is evident that Test 4 experienced remarkably higher signal strengths for a longer period then all other tests.

To get a better understanding of Tests 1-3, it was necessary to view the data within the first 15 hours (Figure 3.14). Figure 3.14 supports the finding that Test 4 endured much higher signal strength than the other tests, but it shows that Test 1 had the lowest of all CSS. Test 1 had the lowest and slowest pressure and rotation cycle, so it has the lowest signal strength. Test 2 and Test 3 had the same setup parameters, so their CSS are close to one another after 8 hours.

Intensity analysis for damage quantification was conducted for each test and compared. Each test was separated into either 3 or 4 sections based on signal strength spikes. The section separations for Test 1, Test 2, Test 3, and Test 4 can be found in Figures 3.15, 3.16, 3.17, and 3.18, respectively. Note that S1, S2, S3, S4 are the notations for Section 1, Section 2, Section 3, and Section 4, respectively.

Each of these sections were assigned a severity and historic index based on the formulas provided in the literature review (Eq. 1.1 & 1.2). The entire data set for each test was also assigned a severity and historic index (seen on Figure 3.19 as “All”). These values can be found on the intensity plot in Figure 3.19.

The intensity plot was split into three different areas depending on level of damage occurred, those being: minimal damage, crack initiation and propagation, and failure. The intensity values of less damage are plotted near the bottom left of the plot while the values of high damage are found in the top right corner. It is seen that the historic index for sections 2 and 3 of all tests is higher than section 4 of the respective test. Sections 2 and 3 are in the middle of the tests and are where crack propagates. Section 4 is at the end of the tests and is where failure of the bearing happens. This points to the conclusion that crack initiation and propagation has a greater severity and historic index then at failure of the bearing.

The coefficient of variance was calculated for all parameters pertinent to analysis. The coefficient of variance is calculated by dividing the standard deviation by the mean of all sensors that had a response to the same hit. The parameters pertinent to analysis are historic index, signal strength, amplitude, absolute energy, frequency centroid, and peak frequency. The coefficient of variance of all these parameters can be seen in Table 3.3.

Table 3.1 Setup per Test

	Test 1	**Test 2**	**Test 3**	**Test 4**
Running Time	25.8 hours	16.9 hours	15.15 hours	38.01 hours
Pressure	625 psi	1250 psi	1250 psi	1875 psi
Rotation Cycle	10Hz, 15Hz, 20Hz every minute	15Hz, 20Hz every two minutes	15Hz, 20Hz every two minutes	15Hz, 20Hz every two minutes
Picture Timing	After Failure	After Failure	After Failure	After major spikes in data

Table 3.2 Cluster Waveforms and Continuous Wavelet Transform

	Waveform	Continuous Wavelet Transform
Cluster 0	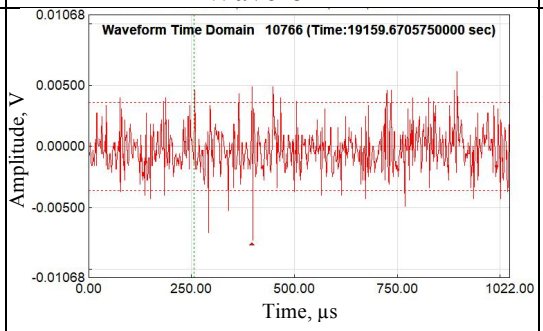	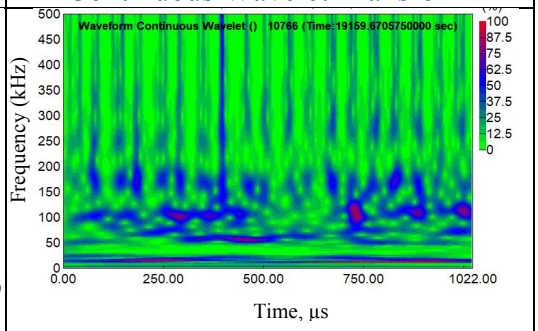
Cluster 1	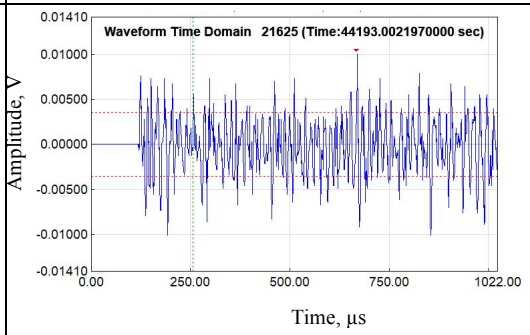	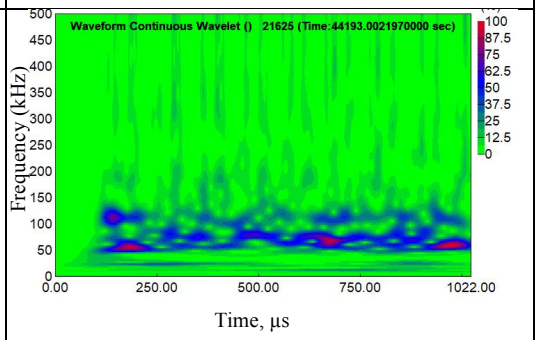
Cluster 2	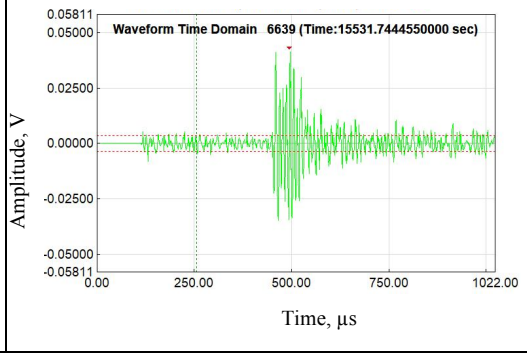	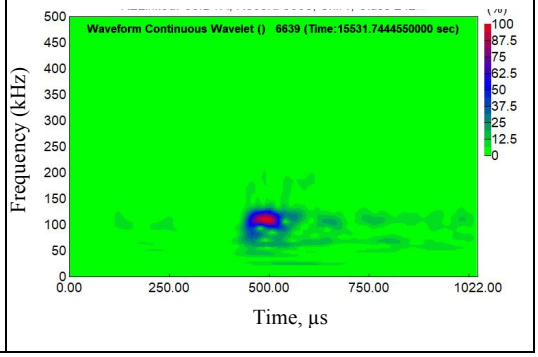

Table 3.3 Coefficient of Variance

	Coefficient of Variance
Historic Index	9.11%
Signal Strength	4.36%
Amplitude	1.52%
Absolute Energy	4.51%
Frequency Centroid	1.11%
Peak Frequency	1.71%

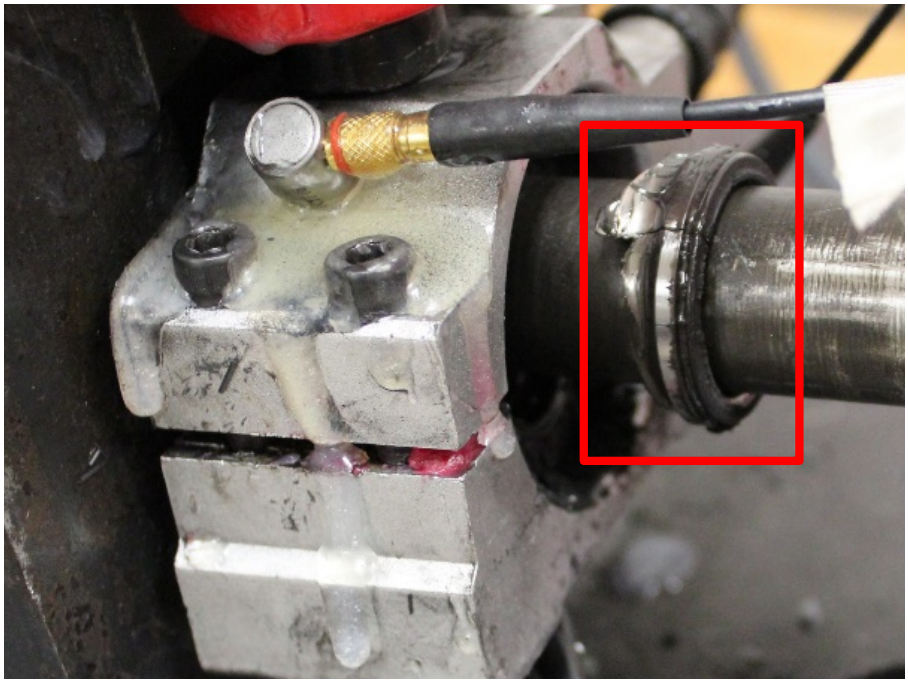

Figure 3.1 Test 1 Bearing Failure

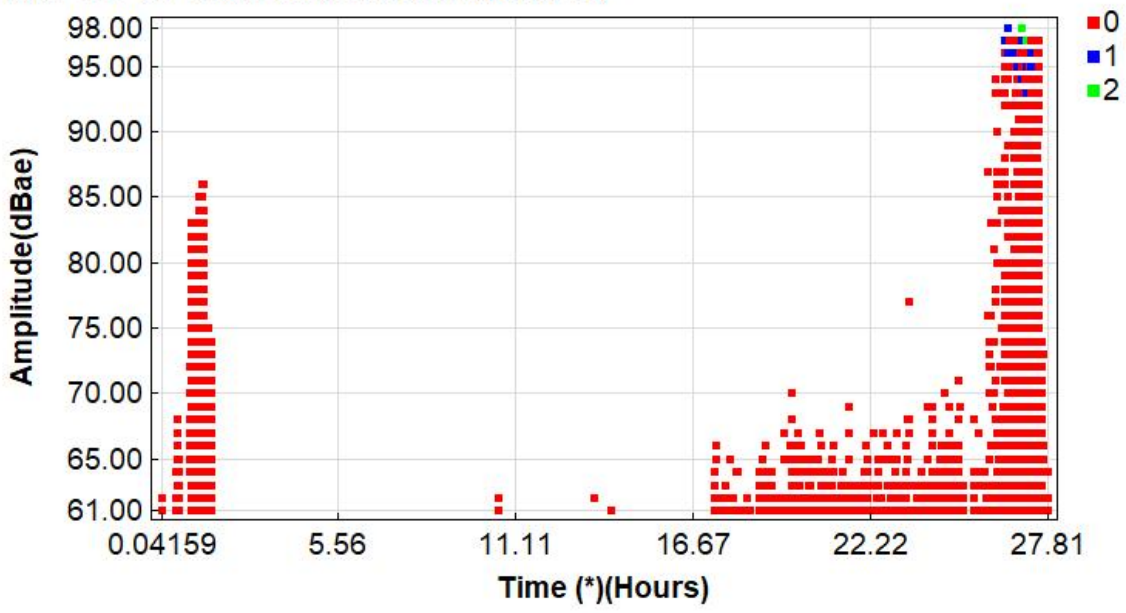

Figure 3.2 Test 1 Amplitude vs Time

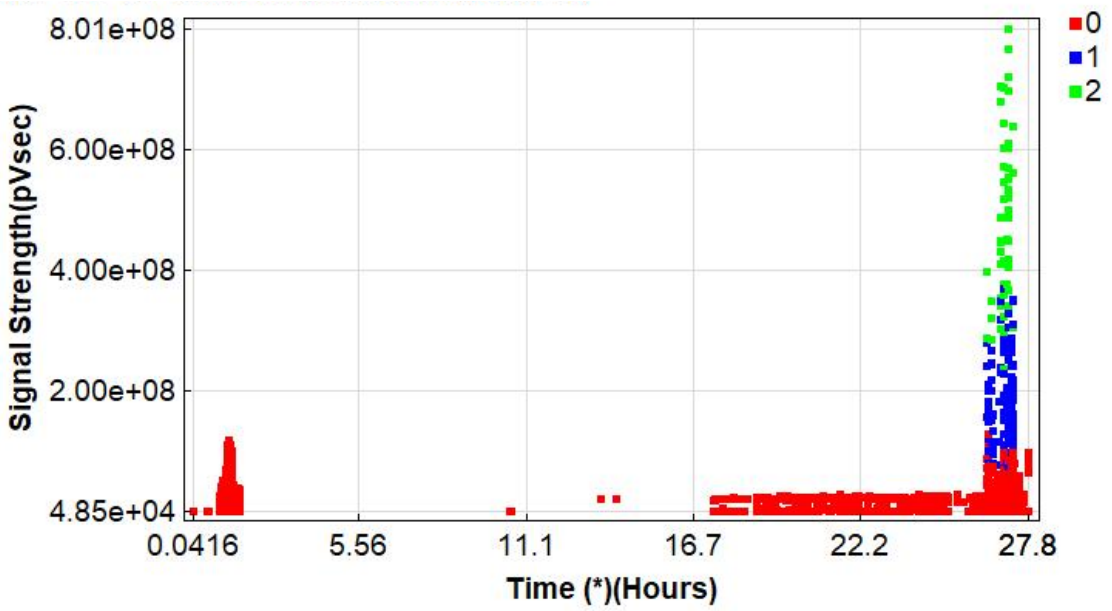

Figure 3.3 Test 1 Signal Strength vs Time

Figure 3.4 Test 2 Bearing Failure

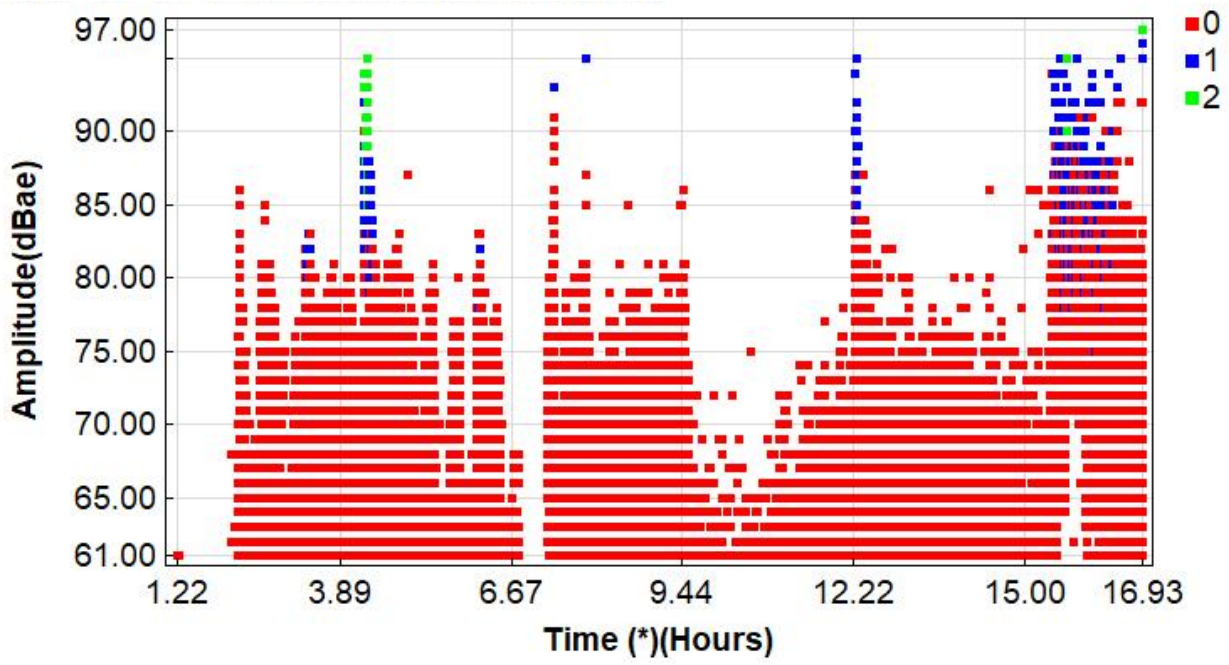

Figure 3.5 Test 2 Amplitude vs Time

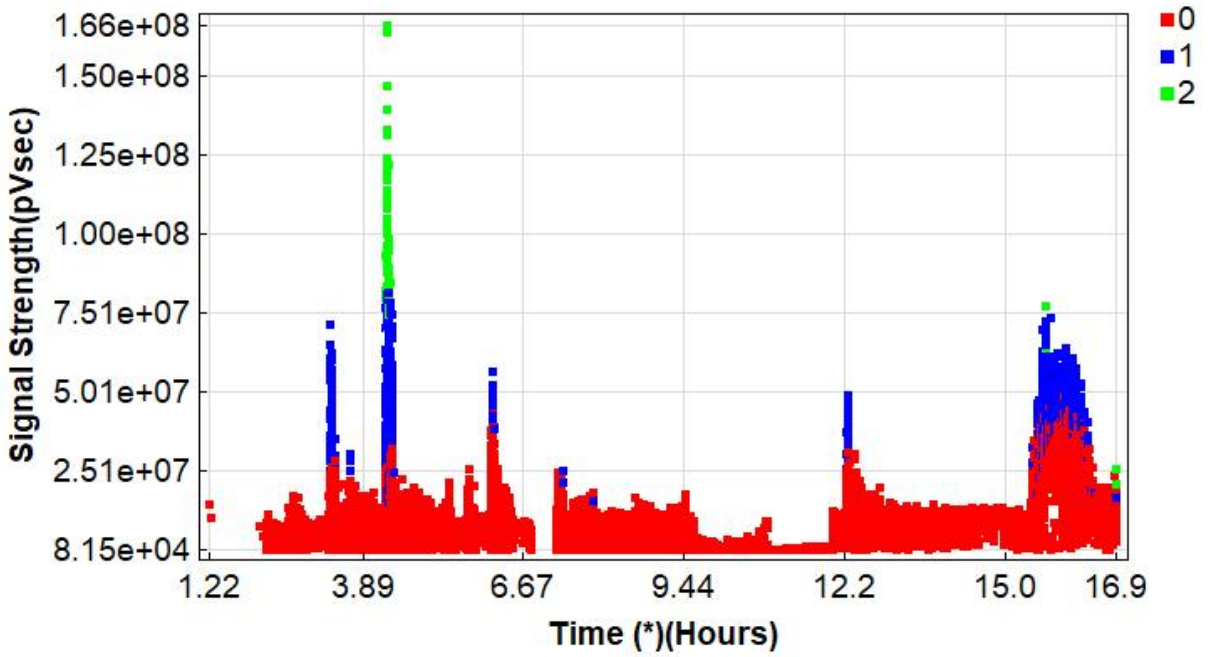

Figure 3.6 Test 2 Signal Strength vs Time

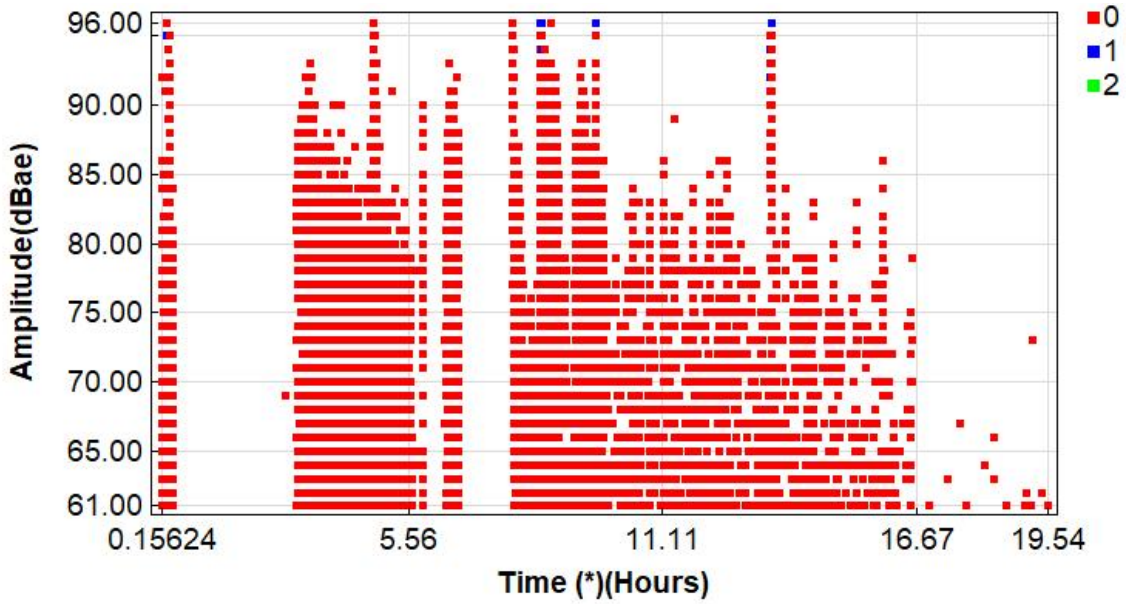

Figure 3.7 Test 3 Amplitude vs Time

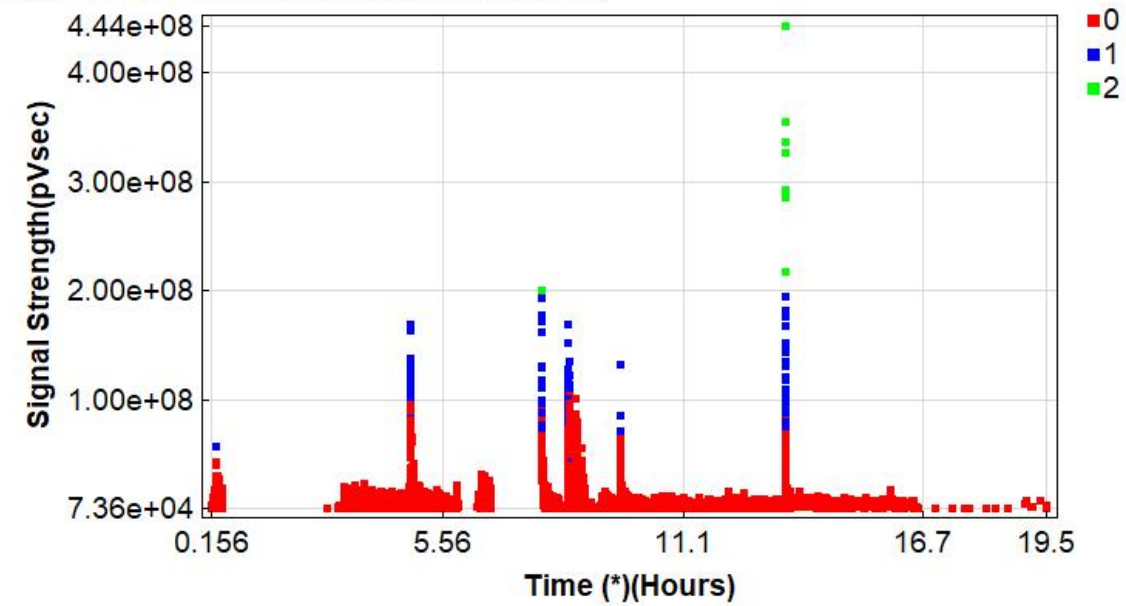

Figure 3.8 Test 3 Signal Strength vs Time

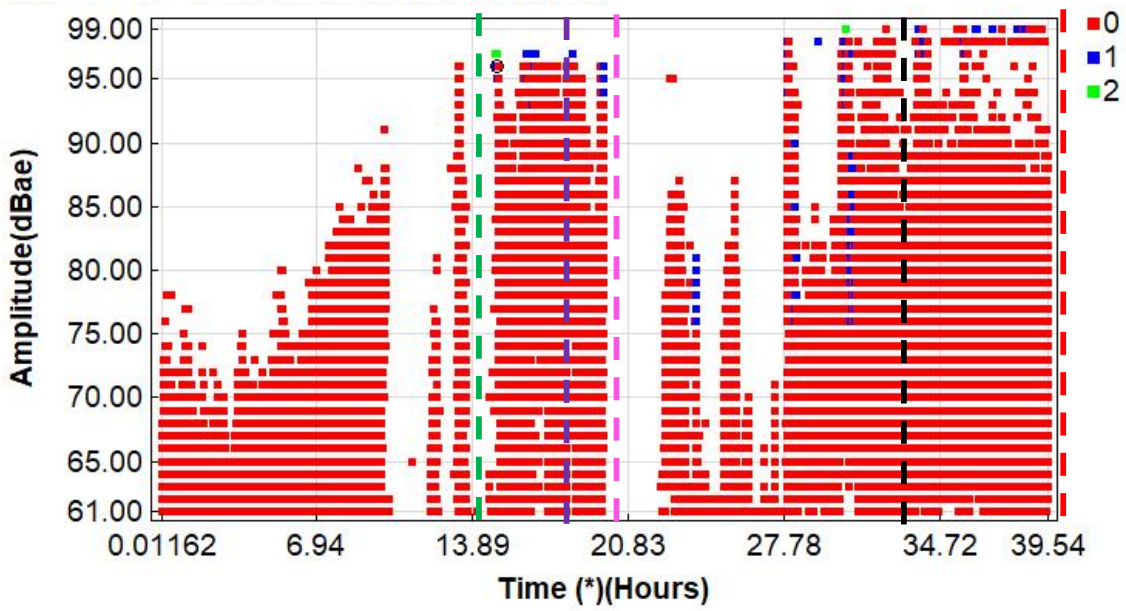

Figure 3.9 Test 4 Amplitude vs Time

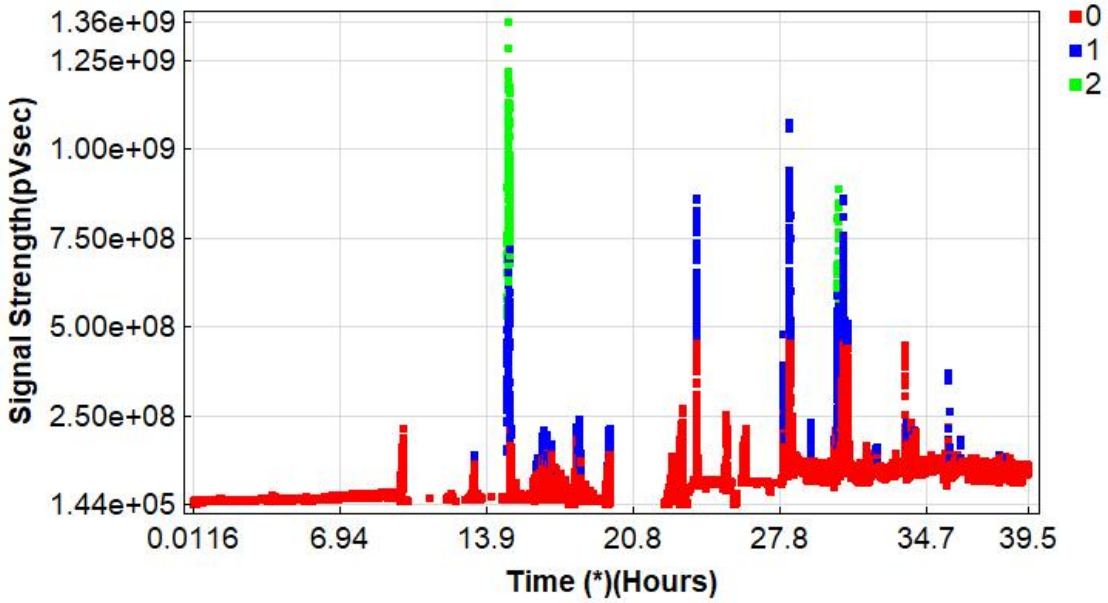

Figure 3.10 Test 4 Signal Strength vs Time

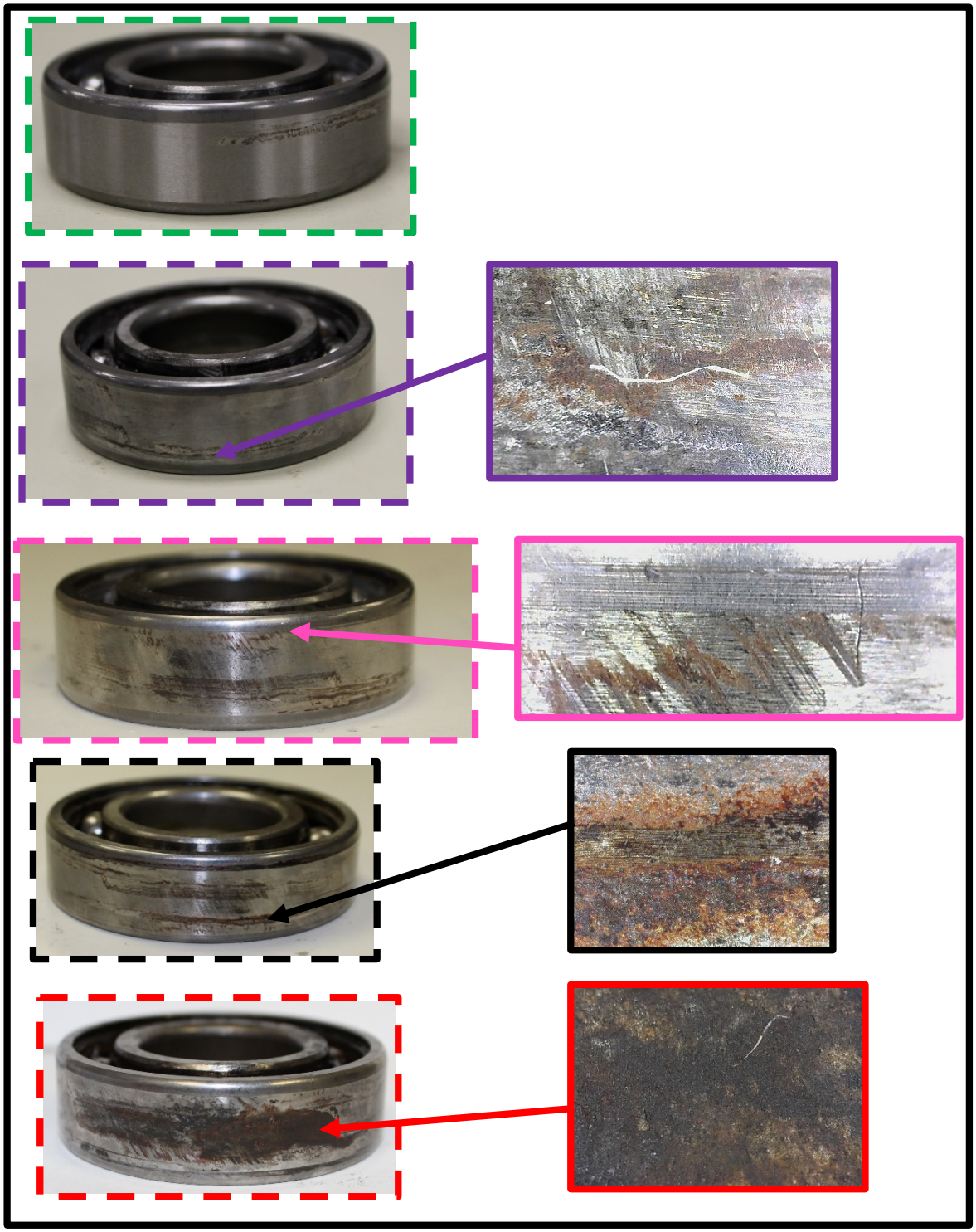

Figure 3.11 Intermediate Bearing Images

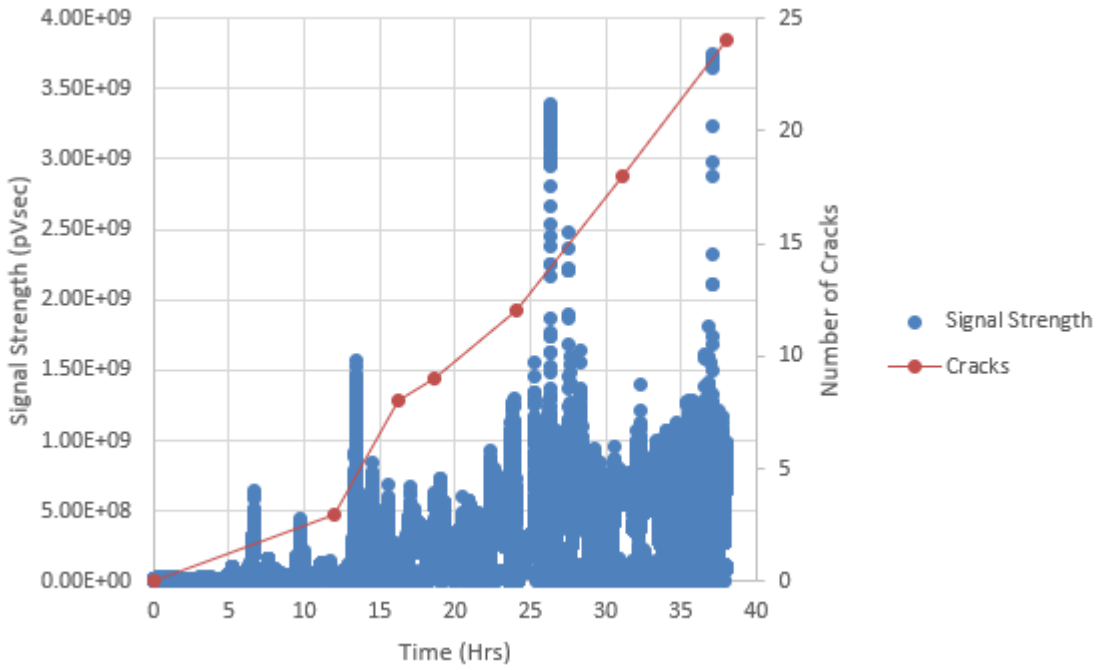

Figure 3.12 Test 4 Number of Cracks and Signal Strength vs Time

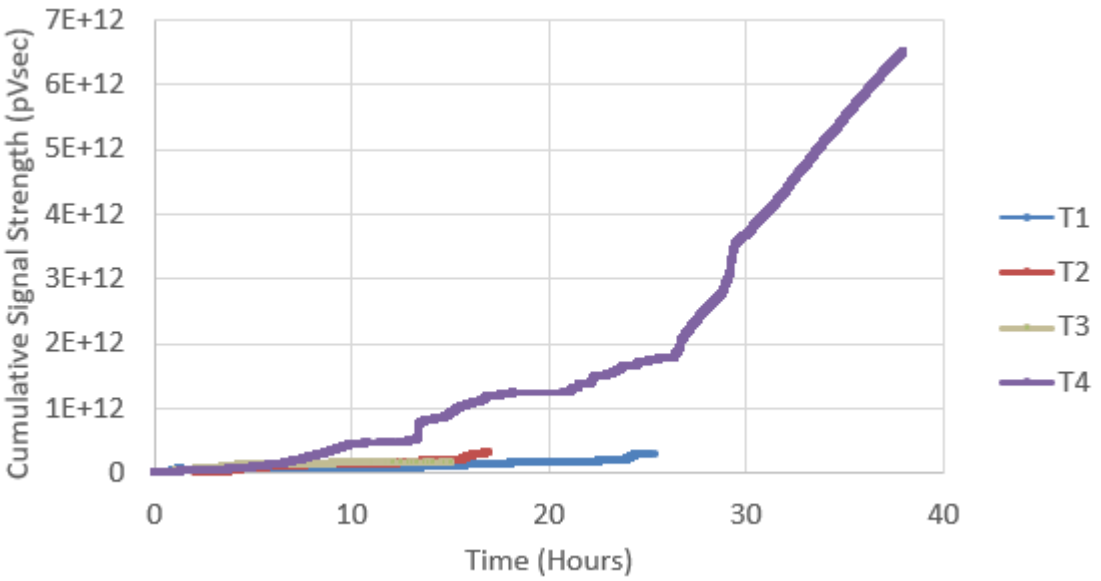

Figure 3.13 Cumulative Signal Strength for all Tests

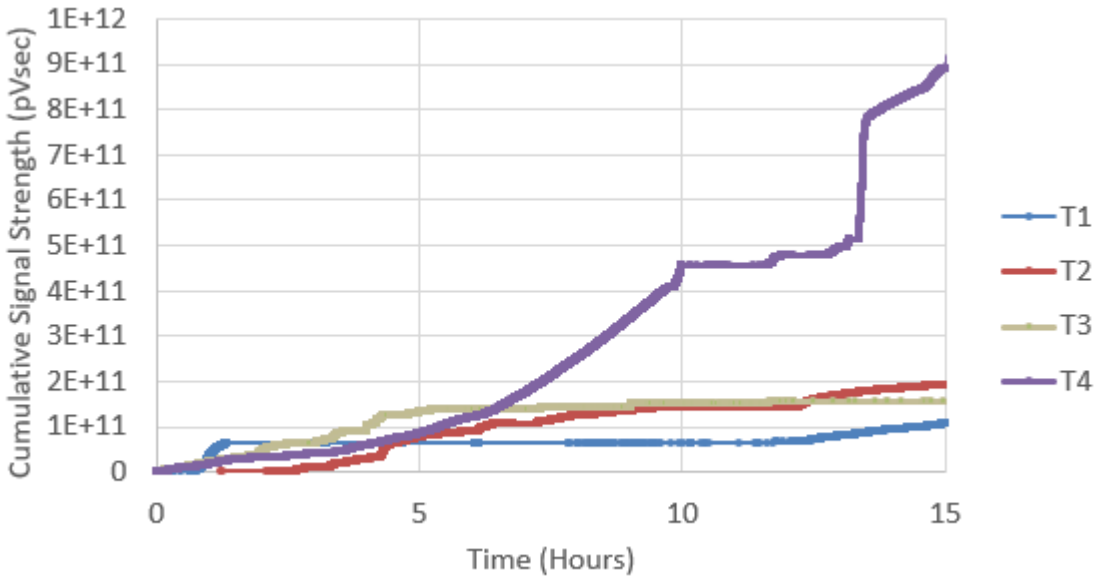

Figure 3.14 Cumulative Signal Strength for all Tests Hours 1-15

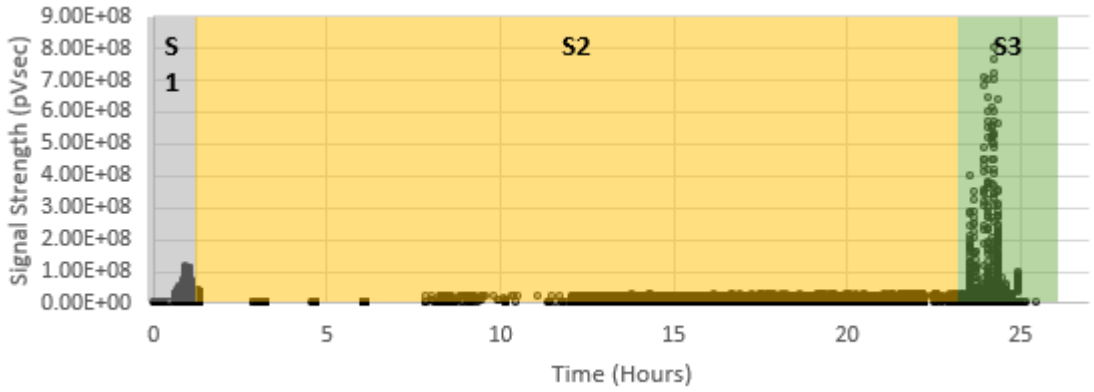

Figure 3.15 Test 1 Signal Strength vs Time in Sections

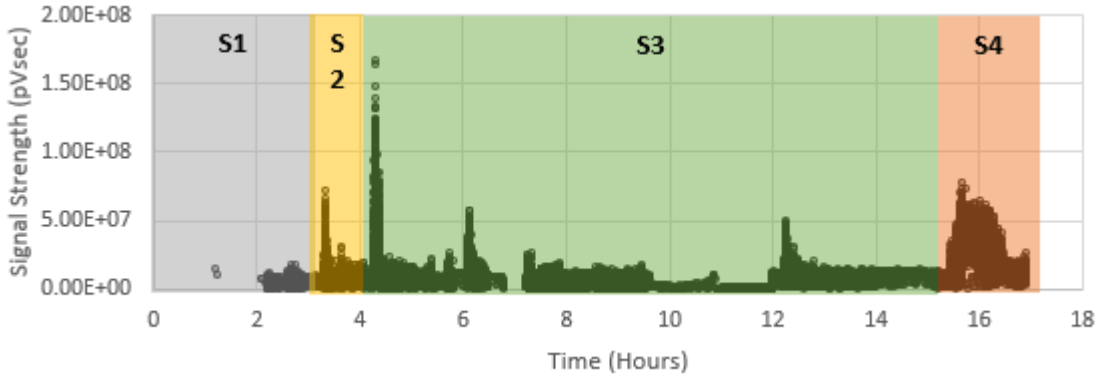

Figure 3.16 Test 2 Signal Strength vs Time in Sections

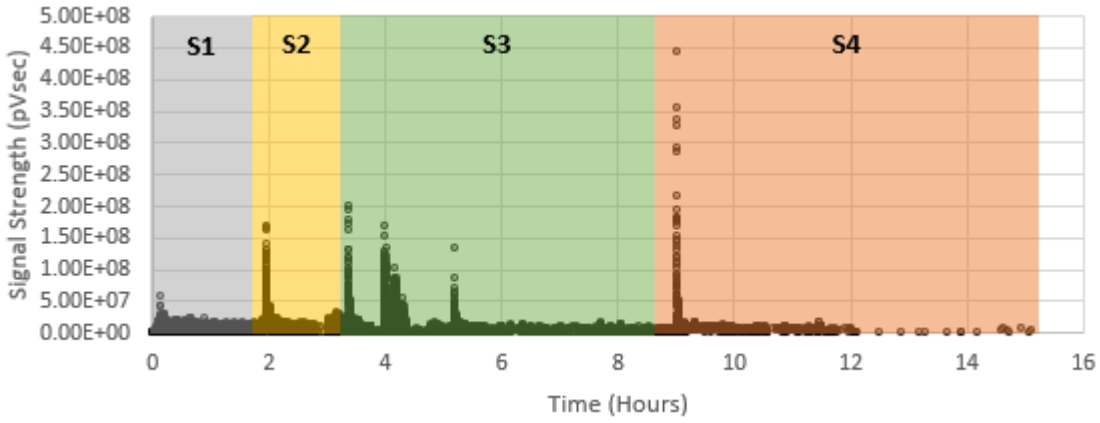

Figure 3.17 Test 3 Signal Strength vs Time in Sections

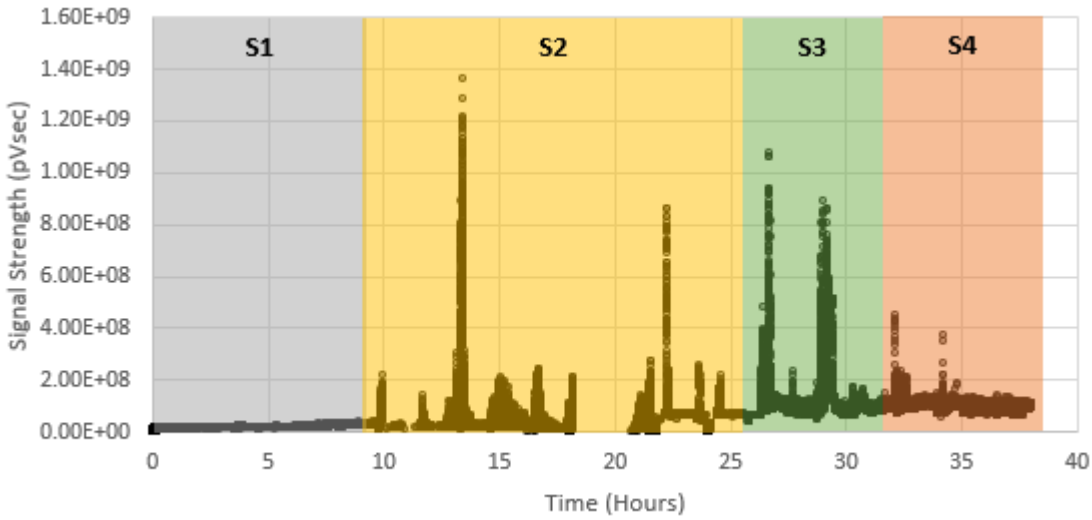

Figure 3.18 Test 4 Signal Strength vs Time in Sections

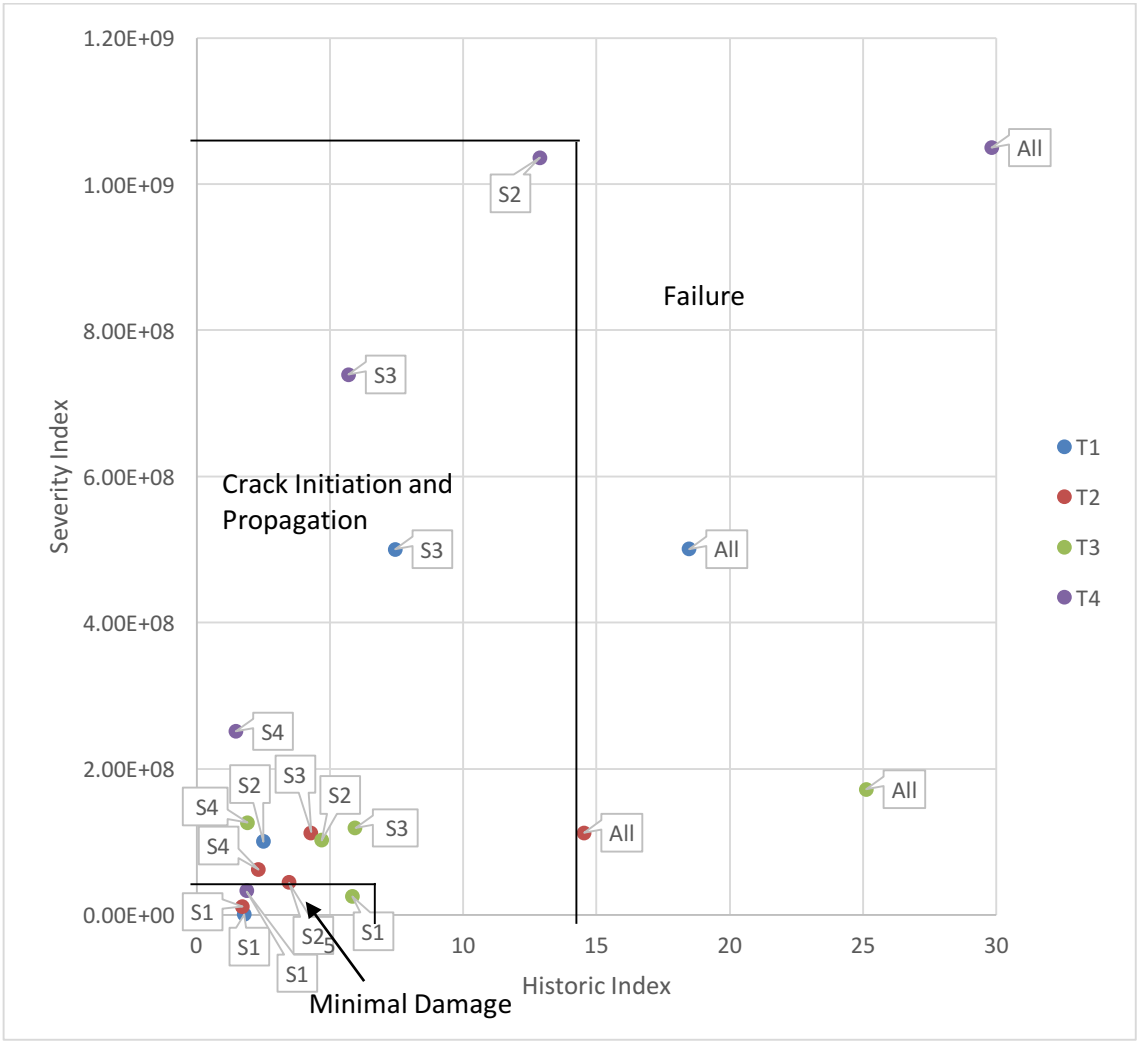

Figure 3.19 Intensity Plot for all Tests

CHAPTER 4

CONCLUSION

4.1 Summary

Rolling element bearings are pivotal to most all rotating machinery. Quality performance of rolling element bearings are necessary to ensure the machine does what it is intended for. To prevent degradation to machine performance and unexpected system failure, bearing fault diagnosis and prognosis must be used. Acoustic emission monitoring is a technique which can assess and evaluate bearing condition. The testing done focused on nondestructively monitoring the crack growth in rolling element bearings in a marine environment and determining the acoustic emission parameters which embody crack initiation and propagation.

Four rolling element bearings were tested in a specially made rotating machine test bed. The rotating machine test bed ensures that a bearing may be rotated at high speeds in various cycles while enduring a downward force of up to 4000 pounds through a hydraulic system. Acoustic emission data was collected for each bearing. The first bearing was tested with a load of 625psi with a rotation cycle of 1 minute at the following rates: 10Hz, 15Hz, and 20Hz. The next two bearings were tested with a load of 1250psi with a rotation cycle of 2 minutes at 15Hz and then 2 minutes at 20Hz. The last bearing was tested with a load of 185psi with a rotation cycle of 2 minutes at 15Hz and then 2 times at 20Hz. This change in load and rotation cycle was done in order to accelerate the degradation process.

4.2 Conclusions

Several Conclusions were drawn from this experiment:

- The AE data was separated into three clusters using k-means unsupervised pattern recognition method with distance type of Euclidean. Two clusters are categorized as relatively indistinct. The other cluster is related to damage initiation and growth

due to the localized event in terms of time and frequency of the CWT, and a quality wave form. The clustering method used successfully classified crack initiation and propagation.

- Useful AE parameters for classifying crack propagation are:
    - amplitude (above 90 dB),
    - initiation frequency (below 20000 kHz),
    - absolute energy (above 1E7 J),
    - frequency centroid (below 215 kHz),
    - peak frequency (below 150 kHz), and
    - signal strength (above 5E7 pVsec).
- Signal strength was a useful parameter in understand the progression of damage. Three to four sections were defined based on spikes in signal strength. It was determined that the severity index and historic index at crack initiation and propagation is much higher than at the final section where failure occurred.
- AE is suitable for remote monitoring of bearing degradation. With the use of signal alarms based upon the clustering method and parameters discussed, one can be notified when a crack is propagating and prepare for failure of the bearing.

REFERENCES

Abdelrahman, M. A. (2016). Evaluation of Concrete Degradation Using Acoustic Emission: Data Filtering And Damage Detection.

Anastasopoulos, A. (2005). Pattern recognition techniques for acoustic emission based condition assessment of unfired pressure vessels. *Journal of Acoustic Emission*, *23*, 318.

Anay, R., Cortez, T. M., Jáuregui, D. V., ElBatanouny, M. K., & Ziehl, P. (2016). On-site acoustic-emission monitoring for assessment of a prestressed concrete double-tee-beam bridge without plans. Journal of Performance of Constructed Facilities, 30(4), 04015062.

ASTM E1316. 2006. Standard Terminology for Nondestructive Examinations. American Standard for Testing and Materials, 1-33.

Baby, S., Kumar, J., Kumar, M., & Kumar, V. (2006). Application of NDE techniques for damage measurements in IMI-834 titanium alloy under monotonic loading conditions. In *Proc. National Seminar on Non-Destructive Evaluation* (pp. 347-356).

Baccar, D., & Söffker, D. (2015). Wear detection by means of wavelet-based acoustic emission analysis. *Mechanical Systems and Signal Processing*, *60*, 198-207.

Boczar, T., & Lorenc, M. (2004). Determining the repeatability of acoustic emission generated by the hsu-nielsen calibrating source. *Molecular and quantum Acoustics*, *25*, 177-192.

Cerrada, M., S´anchez, R.-V., Li, C., Pacheco, F., Cabrera, D., de Oliveira, J. V., & V´asquez, R. E. (2018). A review on data-driven fault severity assessment in rolling bearings. Mechanical Systems and Signal Processing *, 99*(VOL) ,169–196.

Cover, T. M., & Hart, P. (1967). Nearest neighbor pattern classification. *IEEE transactions on information theory*, *13*(1), 21-27.

Drummond, G., Watson, J. F., & Acarnley, P. P. (2007). Acoustic emission from wire ropes during proof load and fatigue testing. *Ndt & E International*, *40*(1), 94-101.

ElBatanouny, M. K. (2012). *Implementation of acoustic emission as a non-destructive evaluation method for concrete structures* (Doctoral dissertation, University of South Carolina).

ElBatanouny, M. K., Ziehl, P. H., Larosche, A., Mangual, J., Matta, F., & Nanni, A. (2014). Acoustic emission monitoring for assessment of prestressed concrete beams. *Construction and building materials*, *58*, 46-53.

Farhidzadeh, A., Mpalaskas, A. C., Matikas, T. E., Farhidzadeh, H., & Aggelis, D. G. (2014). Fracture mode identification in cementitious materials using supervised pattern recognition of acoustic emission features. *Construction and building materials*, *67*, 129-138.

Fiala, J., Mazal, P., & Kolega, M. (2011). Cycle induced microstructural changes. *International Journal of Microstructure and Materials Properties*, *6*(3-4), 259-272.

Fowler, T., Blessing, J., and Conlisk, P. (1989). "New Directions in Testing." Proc. 3rd International Symposium on AE from Composite Materials, Paris, France.

Georgoulas, G., Loutas, T., Stylios, C. D., & Kostopoulos, V. (2013). Bearing fault detection based on hybrid ensemble detector and empirical mode decomposition. *Mechanical Systems and Signal Processing*, *41*(1-2), 510-525.

Golaski, L., Gebski, P., & Ono, K. (2002). Diagnostics of reinforced concrete bridges by acoustic emission. *Journal of acoustic emission*, *20*(2002), 83-89.

Gutkin, R., Green, C. J., Vangrattanachai, S., Pinho, S. T., Robinson, P., & Curtis, P. T. (2011). On acoustic emission for failure investigation in CFRP: Pattern recognition and peak frequency analyses. *Mechanical systems and signal processing*, *25*(4), 1393-1407.

Hamrock, B. J., Schmid, S. R., & Jacobson, B. O. (2004). *Fundamentals of fluid film lubrication*. CRC press.

Immovilli, F., Cocconcelli, M., Bellini, A., & Rubini, R. (2009). Detection of generalized-roughness bearing fault by spectral-kurtosis energy of vibration or current signals. *IEEE Transactions on Industrial Electronics*, *56*(11), 4710-4717.

Jemielniak, K. (2001). Some aspects of acoustic emission signal pre-processing. Journal of Materials Processing Technology, 109(3), 242-247.

Kateris, D., Moshou, D., Pantazi, X. E., Gravalos, I., Sawalhi, N., & Loutridis, S. (2014). A machine learning approach for the condition monitoring of rotating machinery. *Journal of Mechanical Science and Technology*, *28*(1), 61-71.

Kumar, C. S., Arumugam, V., Sengottuvelusamy, R., Srinivasan, S., & Dhakal, H. N. (2017). Failure strength prediction of glass/epoxy composite laminates from

acoustic emission parameters using artificial neural network. Applied Acoustics, 115, 32-41.

Liang, C. C., Lai, W. H., & Hsu, C. Y. (1998). Study of the nonlinear responses of a submersible pressure hull. International journal of pressure vessels and piping, 75(2), 131-149.

Likas, A., Vlassis, N., and Verbeek, J. J. (2003). The global k-means clustering algorithm. *Pattern recognition,* 36(2), 451-461.

Lovejoy, S. C. (2008). Acoustic emission testing of beams to simulate SHM of vintage reinforced concrete deck girder highway bridges. *Structural Health Monitoring*, *7*(4), 329-346.

Mangual, J., ElBatanouny, M., Ziehl, P., & Matta, F. (2012). Corrosion damage quantification of prestressing strands using acoustic emission. *Journal of Materials in Civil Engineering*, *25*(9), 1326-1334.

Mazal, P., Pazdera, L., & Dvořáček, J. (2011). Application of acoustic emission method in contact damage identification. *International Journal of Materials & Product Technology*, *41*(1), 140-152.

McFadden, P. D., & Smith, J. D. (1985). The vibration produced by multiple point defects in a rolling element bearing. *Journal of sound and vibration*, *98*(2), 263-273.

McInerny, S. A., & Dai, Y. (2003). Basic vibration signal processing for bearing fault detection. *IEEE Transactions on education*, *46*(1), 149-156.

Mitra, P., Murthy, C. A., & Pal, S. K. (2002). Unsupervised feature selection using feature similarity. *IEEE transactions on pattern analysis and machine intelligence*, *24*(3), 301-312.

Murav'ev, T. V., & Zuev, L. B. (2008). Acoustic emission during the development of a Lüders band in a low-carbon steel. *Technical Physics*, *53*(8), 1094-1098.

Niu, G., Zhang, B., Ziehl, P., Ferrese, F., & Golda, M. (2019, September). Rolling Element Bearing Fault Diagnosis Based on Deep Belief Network and Principal Component Analysis. In Proceedings of the Annual Conference of the PHM Society (Vol. 11, No. 1).

PCI-2 – PCI-Based Two-Channel AE Board & System. (2007, April 11). Retrieved from https://www.physicalacoustics.com/by-product/pci-2/.

Raj, B., Jayakumar, T., & Thavasimuthu, M. (2002). *Practical non-destructive testing*. Woodhead Publishing.

Ramasso, E., Placet, V., & Boubakar, M. L. (2015). Unsupervised consensus clustering of acoustic emission time-series for robust damage sequence estimation in composites. *IEEE Transactions on Instrumentation and Measurement*, *64*(12), 3297-3307.

Schultz, Arturo E.; Morton, Daniel L.; Tillmann, Anton S.; Campos, Javier E.; Thompson, David J.; Lee-Norris, Alexandria J.; Ballard, Ryan M.. (2014). Acoustic Emission Monitoring of a Fracture-Critical Bridge. Minnesota Department of Transportation Research Services & Library. Retrieved from the University of Minnesota Digital Conservancy, http://hdl.handle.net/11299/163209.

Shahidan, S., Pulin, R., Bunnori, N. M., & Holford, K. M. (2013). Damage classification in reinforced concrete beam by acoustic emission signal analysis. Construction and Building Materials, 45, 78-86.

Shahiron, S., Bunnori, N. M., Noorsuhada, M. N., & Basri, S. R. (2012). Health index evaluation on acoustic emission signal for concrete structure by intensity analysis method. In *Advanced Materials Research* (Vol. 403, pp. 3729-3733). Trans Tech Publications.

Stack, J. R., Habetler, T. G., & Harley, R. G. (2004). Fault classification and fault signature production for rolling element bearings in electric machines. *IEEE Transactions on Industry Applications*, *40*(3), 735-739.

Tan, C. C. (1990). Application of acoustic emission to the detection of bearing failures. In International Tribology Conference 1990, Brisbane 2-5 December 1990: Putting Tribology to Work; Reliability and Maintainability through Lubrication and Wear Technology; Preprints of Papers (p. 110). Institution of Engineers, Australia.

Tandon, N., & Nakra, B. C. (1990). The application of the sound-intensity technique to defect detection in rolling-element bearings. *Applied Acoustics*, *29*(3), 207-217.

Tinkey, B. V., Fowler, T. J., & Klingner, R. E. (2002). *Nondestructive testing of prestressed bridge girders with distributed damage* (No. FHWA/TX-03/1857-2,).

Xiang, D. (2017, February). Acoustic emission detection of early stages of cracks in rotating gearbox components. In AIP Conference Proceedings (Vol. 1806, No. 1, p. 070010). AIP Publishing LLC.

Xu, J. G. (2008). *Nondestructive evaluation of prestressed concrete structures by means of acoustic emissions monitoring* (Doctoral dissertation).

Yasami, Y., & Mozaffari, S. P. (2010). A novel unsupervised classification approach for network anomaly detection by k-Means clustering and ID3 decision tree learning methods. *The Journal of Supercomputing*, *53*(1), 231-245.

Yoshioka, T., & Fujiwara, T. (1987). Paper II (i) Measurement of propagation initiation and propagation time of rolling contact fatigue cracks by observation of acoustic emission and vibration. In *Tribology Series* (Vol. 12, pp. 29-33). Elsevier.

Zarei, J., & Poshtan, J. (2007). Bearing fault detection using wavelet packet transform of induction motor stator current. *Tribology International*, *40*(5), 763-769.

Zhang, P., Du, Y., Habetler, T. G., & Lu, B. (2010). A survey of condition monitoring and protection methods for medium-voltage induction motors. *IEEE Transactions on Industry Applications*, *47*(1), 34-46.

Zykova, L., Mazal, P., & Pazdera, L. (2006). Identification of contact fatigue stages with acoustic emission method. In *European conference on NDT*.